

IMAGING THE TROPICAL ATLANTIC

***Karl Heinz Szekiolda**

EEC Research Associate

Columbia University

**Author for Correspondence: kszekiolda@ateneo.edu*

ABSTRACT

The equatorial region of the Atlantic is governed by a complex current system that is exposed to high variability at various spatial-temporal scales and is examined with long-time data series. Climatological means and seasons are grouped in order to generate changes at a course time scale. This enables the recognition of major changes at which the major current and atmospheric modulations occur. Correlation maps of various parameters demonstrate that information can be added to climatological maps that cannot be identified with chlorophyll concentrations or temperature alone. Some of the dynamic features in the tropical region may be suppressed even with interannual monthly means. However, observations at higher temporal resolution resolve patchiness of chlorophyll distribution in the presence of westward moving tropical instability waves and eddies that propagate at a velocity of about 22cm sec^{-1} , and have a wavelength averaged at around 350 to 400km. The formation and separation process of eddies from waves take place over a few weeks and was observed with chlorophyll measurements. The mid-summer cooling in the equatorial region concurs with chlorophyll maxima that may range in the average of between 0.3 to 0.45 mg m^{-3} . A second blooming peaks around November to January of the following year and is related to an intermediate light cooling in surface temperature. Long-time observations show that changes in temperature and chlorophyll concentrations appear at various time scales, and data also suggest that a rather large planetary wave with a possible period of about fifteen years passes through the equatorial basin in the Tropical Atlantic. This may cause variations in the thermocline, and parallel to the effects of global temperature increase, multi-decadal modulations are superimposed on the marine environment.

Keywords: *Tropical Atlantic, equatorial currents, chlorophyll, tropical instability waves*

INTRODUCTION

The equatorial region of the Atlantic is governed by a complex current system that consists of large-scale westward currents and eastward counter currents. Related to this complex oceanic system are processes that are responsible for high variability in year-to-year fluctuations that impacts weather pattern and the marine ecosystem at various time-scales. Thus, studies in the Atlantic equatorial regions provide support to applied research, for instance to weather forecasting, and assists to better understand air-sea interaction. The currents in the equatorial region are vital transport systems and have been investigated as shown in the description of the major currents for instance by Bischof *et al.*, (2004), Bonhure *et al.*, (2004) and Gyory *et al.*, (2004). The major surface currents in the Tropical Atlantic include the westward flowing North Equatorial Current, the eastward flowing North Equatorial Counter Current, the westward flowing South Equatorial Current, and the eastward flowing South Equatorial Counter Current. The North Equatorial Current in the Atlantic is located at around 7°N to about 20°N and is in response to the Atlantic trade wind belt, and has a broad westward flow that originates at the NW coast of Africa where it is nourished mainly by the cooler Canary Current. While crossing the Atlantic, the North Equatorial Current entrains waters from the Southern Atlantic into the Northern Atlantic.

Two main modes are observed in the Tropical Atlantic that drive changes, namely the Atlantic Meridional Mode and the North Tropical Atlantic Mode. The Atlantic Meridional Mode develops with a boreal

Research Article

spring intensification of the North Equatorial Counter Current but it is reduced in boreal spring-summer, whereas during the summer season, the Equatorial Under Current and north South Equatorial Current are reinforced. The North Tropical Atlantic Mode usually peaks in boreal spring but can still be observed in summer (Martin-Rey *et al.*, 2023; Amaya *et al.*, 2017; Richter *et al.*, 2013).

The alteration of the upper-ocean circulation during the different seasons and modes was shown to have a decisive role of ocean waves that connect the tropical and equatorial ocean transport (Martin-Rey *et al.*, 2023). Seasonal and interannual variations in the Tropical Atlantic can be followed with sea surface temperature and salinity that have well-defined seasonal cycle within a zonal belt between 5°S to 15°N. The variability in salinity is mostly related to river outflow west of 40° by the Amazon and Orinoco, and to the east, by the Congo in the southern Gulf of Guinea (Dessiera and Dongu, 1994). Aside from river effluents in the region, the salinity in the Equatorial Atlantic is also driven by air-sea interaction and precipitation. Therefore the salt budget shows strong seasonal variations and the freshwater contribution by the Amazon, Congo and Niger develops strong salinity gradients over a wide region. Low salinities are observed during all seasons in the region where the Intertropical Convergence Zone (ITCZ) delivers high precipitation, and in addition to the freshwater supply from the African continent, builds the strong gradient close to the center of the subtropical gyre where evaporation exceeds precipitation (Awo *et al.*, 2018; Gordon *et al.*, 2015). This gradient fluctuates mainly through forcing by the ITCZ, river discharge and rainfall that during its maximum, creates a south-north gradient between the equator and 10°N. In response to the meridional displacement of the ITCZ, the equatorial wind system and equatorial wind anomalies are produced. Changes in the wind system also impact the location and depth of the thermocline or mixed layer. The biological system responds to vertical and horizontal displacement of the thermocline with changes in chlorophyll concentrations (Grodsky *et al.*, 2008, Perez *et al.*, 2004), and wave propagation and upwelling are responsible for variance in chlorophyll concentrations and changes in surface temperature as well.

The South Equatorial Current is a broad, westward flowing current and extends from the surface to a nominal depth of 100 m with its northern boundary at around 4°N. The southern boundary is around 15°S to 25°S, depending on its longitude and season. The southern branch of the South Equatorial Current is fed partly by the northward flowing Benguela Current, and after crossing the Atlantic bifurcates near 16°S, has one branch in northward direction as the North Brazil Current and another weaker branch continues as the Brazil Current (Luko *et al.*, 2021). Part of the North Brazil Current water retroflects and continues as the North Equatorial Counter Current that feeds the northern branch of the South Equatorial Current. Another part of the equatorial current system is the westward flowing Northern South Equatorial Current that is situated between 1°N and the South Equatorial Under Current at 3°S to 5°S, and extends farther north during the boreal winter-spring season. The North Brazil Current carries warm and salty surface water from the South Atlantic waters (Cabr e *et al.*, 2019) and retroflects seasonally near 5°N, while a portion feeds into the North Equatorial Counter Current, and the other part of the North Brazil Current continues northwestward as the Guiana Current (Condie, 1991) that transports relatively fresh surface water occasionally in form of eddies in a northwest direction towards the Caribbean (Fratantoni and Richardson, 2006; Hellweger and Gordon, 2002; Garzoli and Yao 2003; Hu *et al.*, 2004).

This short summary of the complex hydrography of the Tropical Atlantic shows the challenge to explore long-time series of available satellite derived remote sensing data for a survey on surface changes in the Tropical Atlantic. In particular, the access to data that stretch over two decades allows for the analysis of processes that appear at different time-space scales. Therefore, the following study has the objective to update our knowledge on the distribution of selected parameters at various time scales and will emphasize on events that are related to the modification of chlorophyll concentration that is used as a proxy for characterizing the biosphere. Based on the availability of data, the study will subdivide into groupings of climatology, seasons, yearly and monthly observations and analysis of five-day composites of chlorophyll measurements.

Research Article

MATERIALS AND METHODS

The research is based on data selection and image generation with Giovanni, the NASA system for multidisciplinary research and applications that can be accessed via <https://giovanni.gsfc.nasa.gov/> (Liu and Acker 2017; Acker and Leptoukh 2007). The selected parameters are at 4km resolution except for salinity that was operational only for a few years and has a resolution of about 100km. Cloud frequency and salinity data were accessible with Giovanni only at a monthly resolution. For detection of dynamic features, especially for the study of tropical instability waves, a five-day average temporal resolution was chosen for estimating chlorophyll concentrations. In addition, the absorption coefficient a_{dg} was used as a tracer for distinguishing different masses. The coefficient is based on optical signals that are derived from a mixture of phytoplankton, detrital material and chromophoric dissolved organic matter in the water column. Cloud fraction, defined as the number of cloudy pixels divided by the total number of pixels, was displayed with a resolution of one degree.

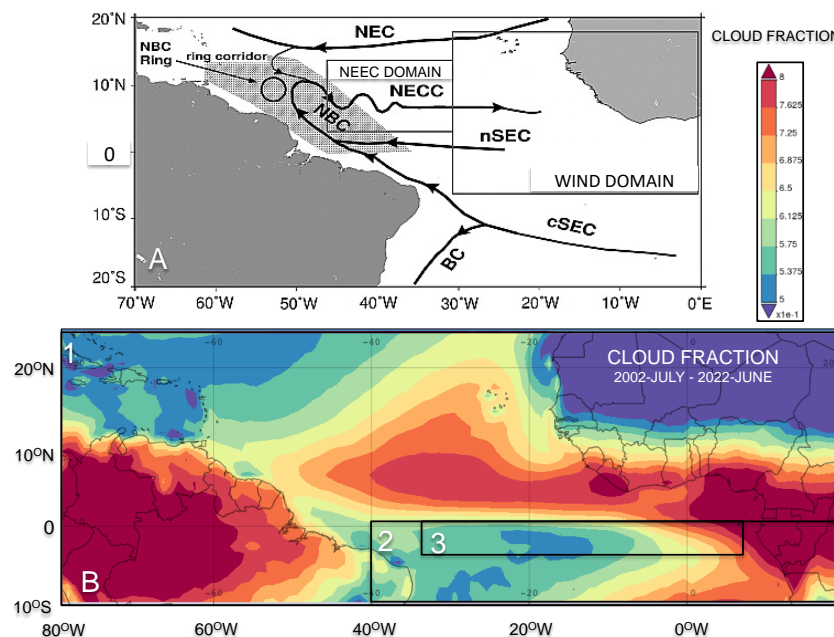


Figure 1: A: Schematic of the current system in the Tropical Atlantic (after Fonseca *et al.*, 2004). B: Cloud fraction defined as the number of cloudy pixels divided by the total number of pixels, based on MODIS-Aqua over July 2002 to June 2022. The color bar on the upper right side gives the estimate of cloud fraction. The areas investigated are: Site 1 covers the area 80°W, 10°S, to 20°E, 25°N; Site 2 covers 40°W, 10°S, to 20°E, 0°N; Site 3 covers 35°W, 3°S, to 4°E, 0°N.

The selected site for this research covers the major current system in the Tropical Atlantic as is shown in Figure 1A. The areas of interest in this research are shown in Figure 1B that also includes the average cloud fraction. As the cloud coverage in the tropics restricts the field of view of any sensor operating in the visible, the average record of high cloud fraction as shown in Figure 1B indicates some of the constraints to obtain space-borne observation in the tropics. Therefore, merging data with a different temporal resolution is frequently required. However, surface features like eddies and meanders appear at different time-space scales compared to the changes of the ITCZ and the related cloud coverage. Thus, some short-lived sea surface phenomena can be accessed only with cloud-free coverage by opportunity because merging observations from different dates may suppress dynamic features that perform at shorter time scales. Merging or mosaicking of data may produce fuzzy images that deviate from reality and can

Research Article

affect and distort statistics. However, five-day composites were found acceptable to resolve some of the dynamic features especially those that are related to tropical instability waves.

RESULTS AND DISCUSSION

Climatological means

Figure 2 shows the high cloud coverage throughout all seasons in the equatorial region. The location and frequency of clouds is related to the northeast and southeast trade winds that converge as a low-pressure zone in the Intertropical Convergence Zone but changes its position and may migrate hundreds of kilometers northwards during boreal spring. This change drives the air-sea interaction on a local scale and the circulation of the Tropical Atlantic Oceans on a basin scale (Waliser and Jiang, 2015). Thus, the interannual variability of the Intertropical Convergence Zone affects the hydro-biological cycles by modifying the current system and the depth of the upper mixed layer and also modifies the marine ecosystem.

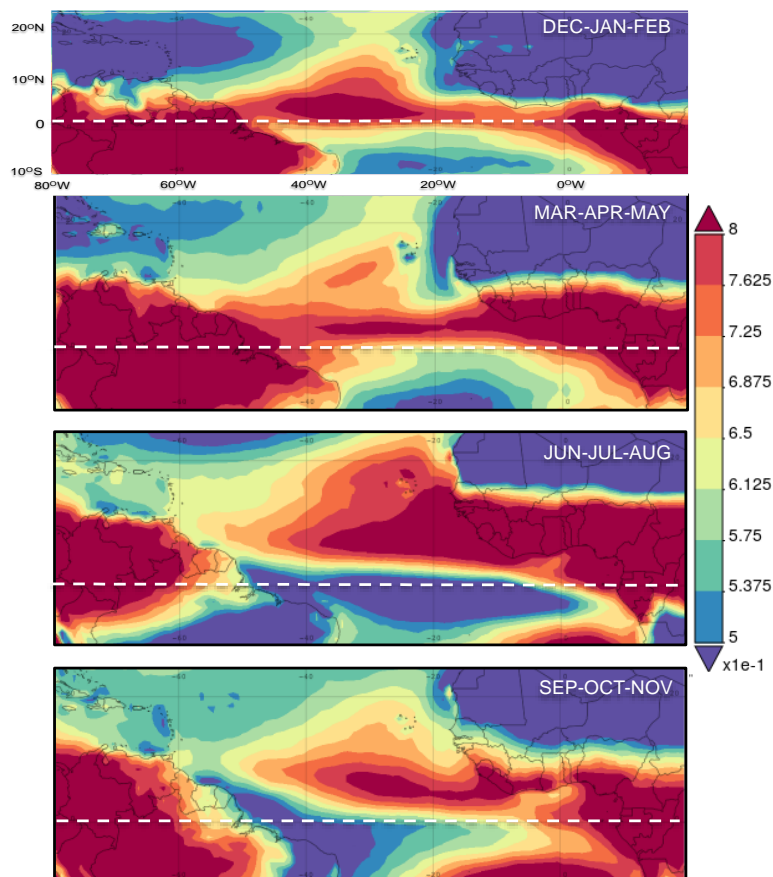


Figure 2: Seasonal average cloud fraction December 2002 to February 2022. The cloud fraction is defined as the number of cloudy pixels divided by the total number of pixels. The white dashed lines in the seasonal images indicate the equator.

The Intertropical Convergence Zone follows the maximum sea surface temperature (Liu *et al.*, 2022) and related atmospheric forcing changes the current dynamics, salinity distribution and vertical exchange processes (Awo *et al.*, 2018). Figure 2 indicates for all seasons high cloud fraction in the equatorial region but a cycle is less pronounced over the ocean compared to the continent. This is attributable to the fact that convection is controlled by surface temperature that changes less over the ocean than over the

Research Article

continent. The cloud fraction displays for all four seasons the highest values north of the equator but the cloud fraction boundary shifts slightly north during the season July to August as is indicated by the area of highest cloud cover. The western part of the Tropical Atlantic has its maximum cloud fraction during the season March to May, and the eastern part shows highest cloud fraction from June to August.

Cloud cover is an indication of precipitation and the connection between low surface salinity values and the position of the ITCZ is evident in Figure 3A. In addition to the contribution of precipitation within the ITCZ region, the contribution of the Orinoco and Amazon in the western part and contributions in the eastern part of the Tropical Atlantic mainly from the Congo, connect the surface water with a low salinity. Equally, the transport of chromophoric dissolved organic matter (or gelbstoff) is related to continental freshwater discharge that can be tracked due to its spectral properties at shorter wavelengths as is shown in Figure 3B with the absorption coefficient a_{dg} (m^{-1}) at $0.443\mu m$.

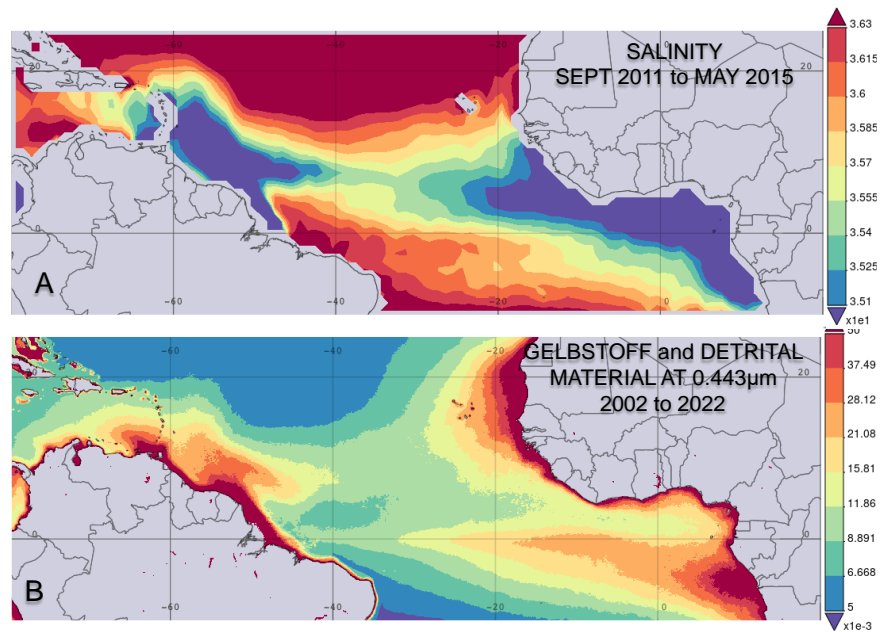


Figure 3: A: Averaged distribution of salinity (psu) for the period September 2011 to May 2015 and B: The absorption coefficient a_{dg} (m^{-1}) at $0.443\mu m$ for 2002 to 2022. a_{dg} is an estimate for the fraction of incident light that is absorbed by gelbstoff, detrital material, and chromophoric dissolved organic matter (CDOM).

The distribution of the absorption coefficient indicates the pathway of detrital material, and chromophoric dissolved organic matter (CDOM) in the surface water. The comparison of Figures 3A and 3B reveals that on the African coast of the Tropical Atlantic the absorption coefficient a_{dg} is not necessarily associated with the transport of freshened water from the Congo alone because along the equatorial regime, the coefficient also responds to planktonic material and its photosynthetic byproducts in the water of the cold tongue. On the western side of the Tropical Atlantic, the low salinity marks the effluents of the Amazon and the Orinoco and both are recognized with absorption coefficients as separate effluents although both may arrive occasionally as a mixture in the Caribbean Sea (Szekielda, 2022).

As convenient as climatological maps are, they suppress most dynamic features and the size and time frame of events to be monitored need appropriate temporal and spatial resolution of observations. Conveniently, observations can be grouped into seasons to generate changes at a course time scale and this procedure would enable the recognition of major changes on a time scale at which current and atmospheric modulations occur.

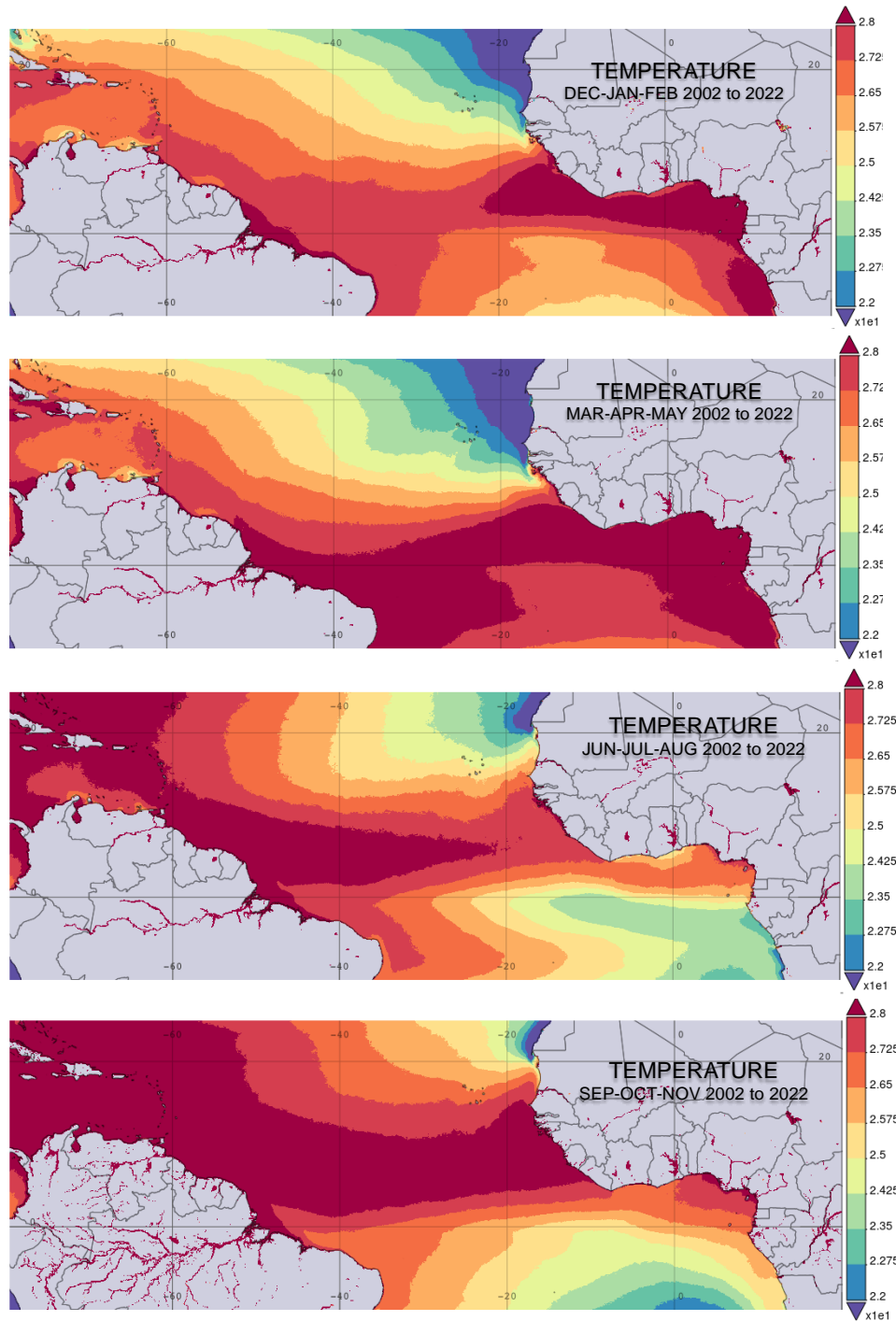


Figure 4: Temperature ($^{\circ}\text{C}$) during seasons based on monthly averaged measurements.

The Tropical Atlantic surface winds are the main force that changes the latitudinal movement of the Inter-Tropical Convergence Zone that establishes a seasonal cycle. Its maximal southern position is in February to April and the maximal northern position is in July to September. Consequently, the air-sea interaction leads also to seasonal changes in the circulation of the upper ocean layer. In the following, changes are documented by grouping the data into seasons for December to February, March to May, June to August

Research Article

and September to November. The seasonal changes of temperature, salinity, chlorophyll, the absorption coefficient a_{dg} and the depth of the mixed layer are displayed in Figures 4 to 12.

Averaging data over almost two decades smooth out details of many dynamic features. However, the different seasons have fundamental distinctions that are shown in Figure 4 with the seasonal temperature changes. The temperatures in December to February indicate upwelling along the NW coast of Africa; but towards the equator, the temperature increases and a warm water tongue extends to about 20°W. The season March to May shows further warming, and upwelling intensifies along the NW coast of Africa compared to the season December to February. Intense warming is observed in the Gulf of Guinea, and along the NW coast of Africa, warming continues and spreads throughout the equatorial region. June to August shows a reduction in the African upwelling regime but the cold tongue south of the equator and along the African coast is well established. The low surface temperature in the eastern equatorial basin is confined to the summer season whereas upwelling along the NW coast of Africa is recognized throughout the whole year although it appears with varying intensity. September to November is the season during which the equatorial trade winds weaken and the sea surface temperature in the eastern basin begins to increase while the western part of the Tropical Equatorial Ocean reaches its maximum temperature.

The changes of salinity distribution follow a seasonal cycle as shown in Figure 5. West of 40°W, changes are mainly related to the river outflow of the Amazon and Orinoco Rivers whereas in the eastern part, the Tropical Atlantic to the Congo River is the main cause for low salinity. Precipitation associated with the displacement of the Intertropical Convergence Zone also controls seasonal variations of salinity as shown by Dessiera and Dongu (1994).

The low salinity during the season December to February is based on reduced fresh water contributions from the Amazon and the Orinoco. April is the season when increase in Amazon effluent extends the low salinity water further north and begins to reach the Lesser Antilles. Large seasonal variability is observed near the mouths of the rivers Amazon, Congo, and Niger whereas between 5°N and 10°N the meridional displacement of the ITCZ is the major driver of variability in salinity (Da-Allada *et al.*, 2013). During the period June to August, the effluent of the Amazon spreads over a large region and the North Brazil Current carries low salinity water from the Amazon region into the Caribbean Sea. September to December are the months when the western part of the Tropical Atlantic warms and freshwater outflow from the Orinoco River increases, and contributes also freshened surface water to the entrance of the Caribbean Sea (Szekielda, 2022; Dessier and Dongu, 1994; Muller-Karger *et al.*, 1988; Hu *et al.*, 2004). Low salinity is observed in November when the North Equatorial Counter Current transports part of the Amazon effluent in an eastward direction. The Congo River during this season is the main source of freshened water in the Guinea Basin and in the average, the surface flow expands in a northwest direction. Hopkins *et al.*, (2013) showed that throughout the year the dispersal of the Congo River plume extends between 400 and 1000 km, northwest along the coastline, or west–southwest out into the open south Atlantic. The extension of low salinity connects during this period with low surface salinity in the western part of the Tropical Atlantic that results in a band of low surface salinities across the Tropical Atlantic.

Figure 6 shows that elevated chlorophyll concentrations are found throughout the year in regions that are characterized by upwelling and river discharge in coastal and adjacent areas, although their intensity may vary throughout the year. Upwelling regions are well developed during all seasons along the Northwest coast of Africa and in the Benguela region whereas eutrophication in the western Tropical Atlantic is mainly related to fresh water discharge from the Amazon and the Orinoco Rivers. The presence of chromophobic dissolved organic matter and suspended sediments in the vicinity of river discharge interferes with the chlorophyll algorithm and therefore it is problematic to define precisely the coastal regions where eutrophication is present. However, the substantial nutrient transport by the Congo, Amazon and Orinoco river plumes is certainly linked to elevated chlorophyll concentrations in coastal waters. Chlorophyll concentrations along the Brazilian coast indicate the retroflexion in the vicinity of the Amazon discharge while part of the current continues as the Guiana Current and transports relatively

Research Article

fresh surface water occasionally in form of eddies in a northwest direction towards the Caribbean Sea (Garzoli *et al.*, 2003; Hu *et al.*, 2004; Fratantoni and Richardson, 2006; Jochumsen *et al.*, 2010).

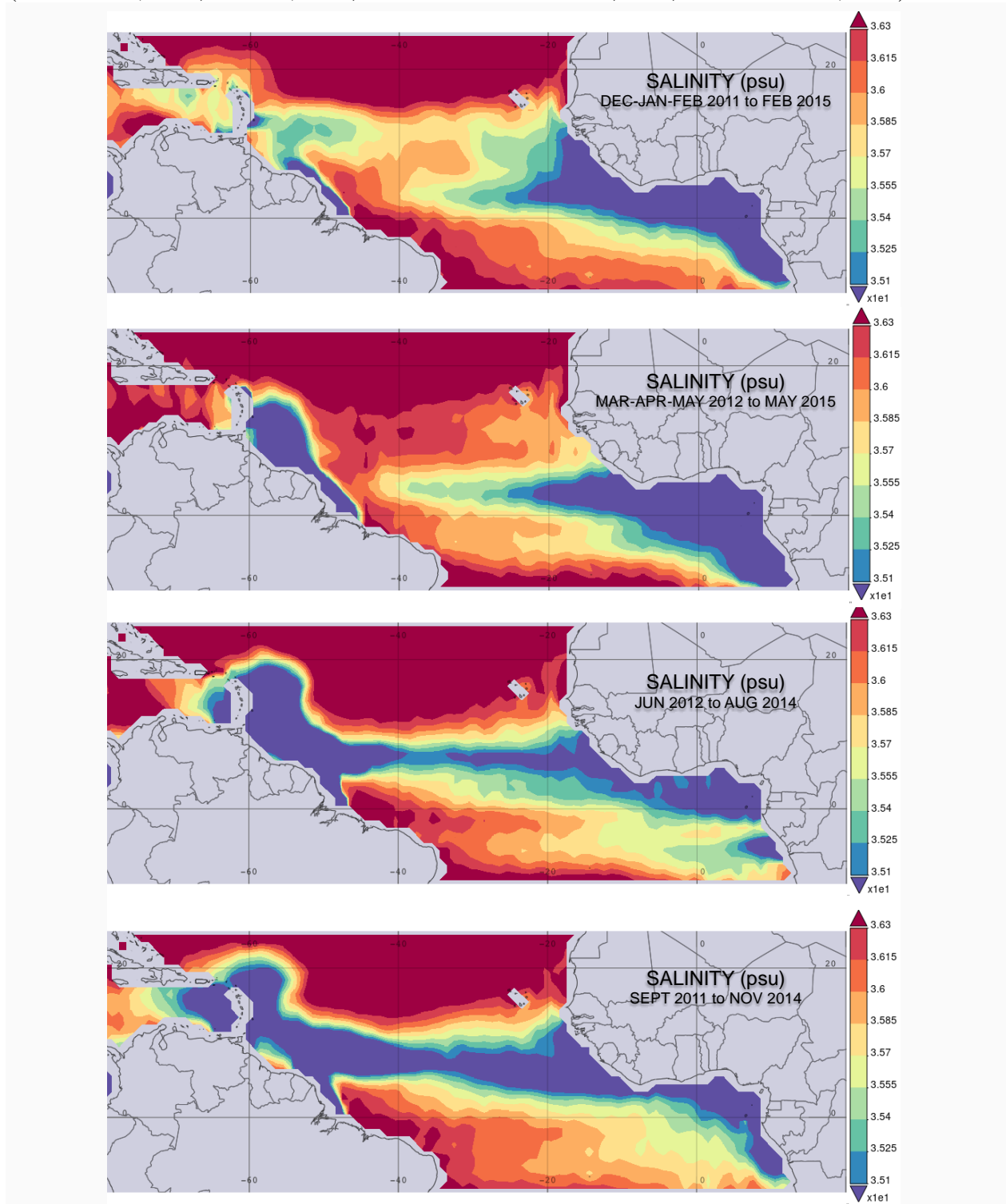


Figure 5: Salinity (psu) during different seasons based on monthly averaged measurements.

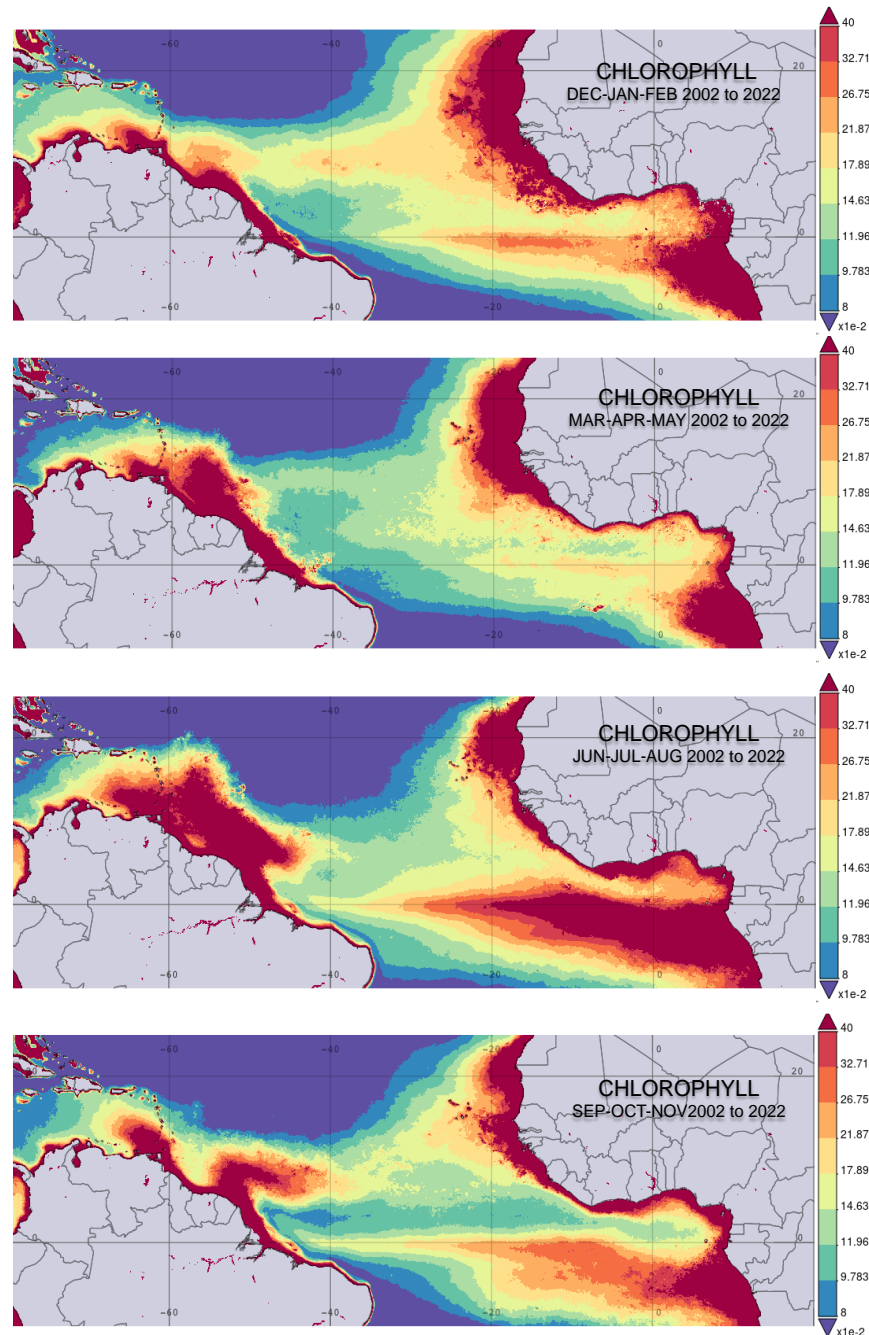


Figure 6: Chlorophyll (mg m^{-3}) during different seasons based on monthly averaged measurements.

During the summer season, from July to August, intense blooming is observed that stretches from the African continent along the equator to about 40° W, and is related to the water temperature of the cold tongue. Upwelling along the northwest coast of Africa is reduced from September to November that can be recognized by increasing temperature and reduced chlorophyll concentrations. On the western part of the basin, from June to November, the outflowing water from the Amazon and the Orinoco shows mixing with the upwelled water along the Venezuelan coast, and at the retroflection, the chlorophyll

Research Article

concentrations build a strong gradient but this gradient is difficult to recognize with surface temperature data.

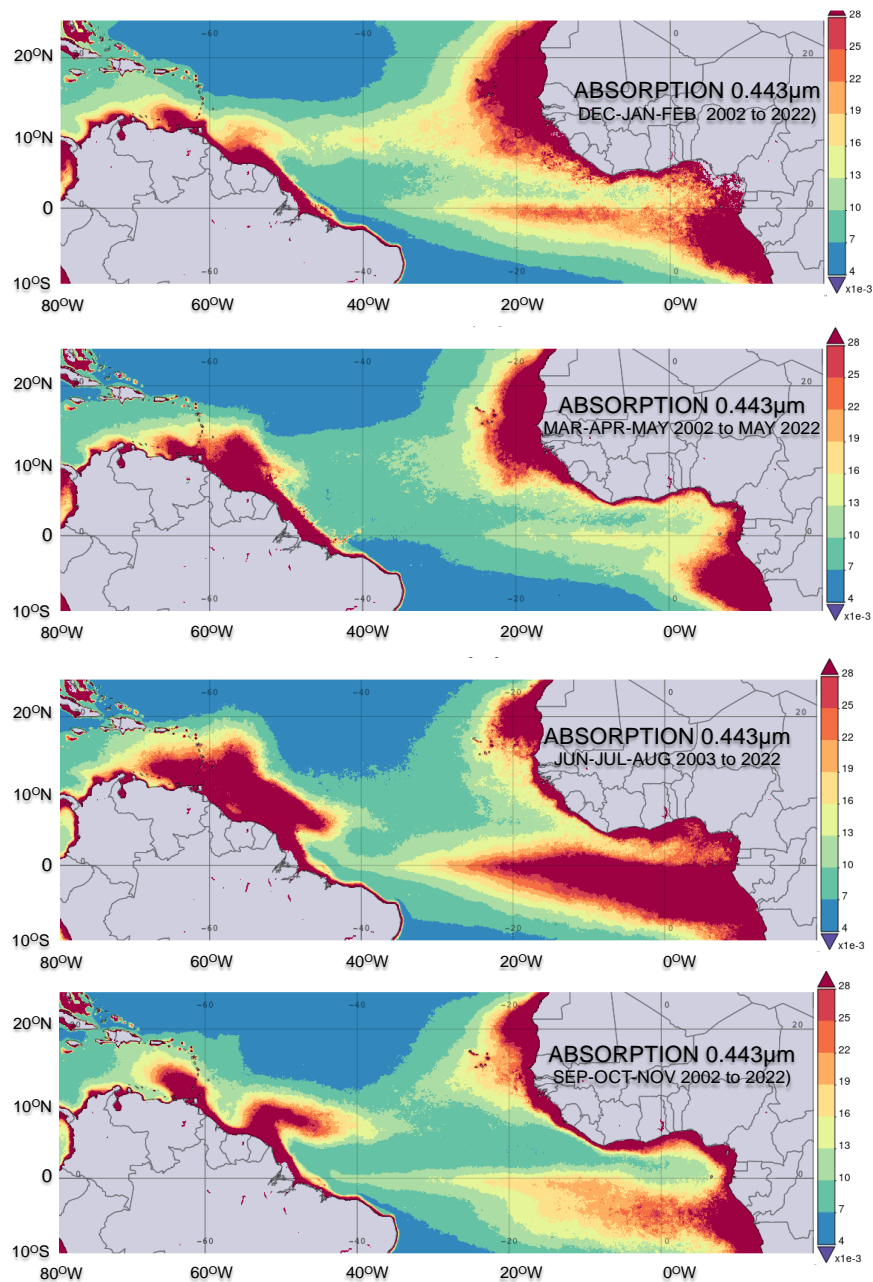


Figure 7: Absorption coefficient a_{dg} (m^{-1}) at $0.443\mu m$ during different seasons based on monthly averaged measurements.

The absorption coefficient a_{dg} at $0.443\mu m$ shown in Figure 7 reveals an almost identical distribution pattern as the chlorophyll concentrations. The similarity is based on the spectral response at $0.443\mu m$ in the open ocean that is dominated mainly by phytoplankton and its metabolic byproducts. In the near-shore waters, detrital material and chromophoric dissolved organic matter affect both parameters as well, as shown in Figure 8A with a comparison of area-averaged chlorophyll concentrations and the absorption

Research Article

coefficient at $0.443\mu\text{m}$, that results in a correlation of $R= 0.78$. However, the scatter diagram of single measurements at 4 km resolution, in Figure 8B, reveals different clusters. Although the correlation coefficient of $R= 0.72$ is still high, the clusters demonstrate the problematic identification of setting boundaries between waters that carry dissolved and particulate inorganic and organic matter (Case 2 water) and those that carry chlorophyll containing phytoplankton only (Case 1 water). Therefore, regional differences in chlorophyll concentrations should take into account a subdivision of the marine ecosystems with additional spectrometric information.

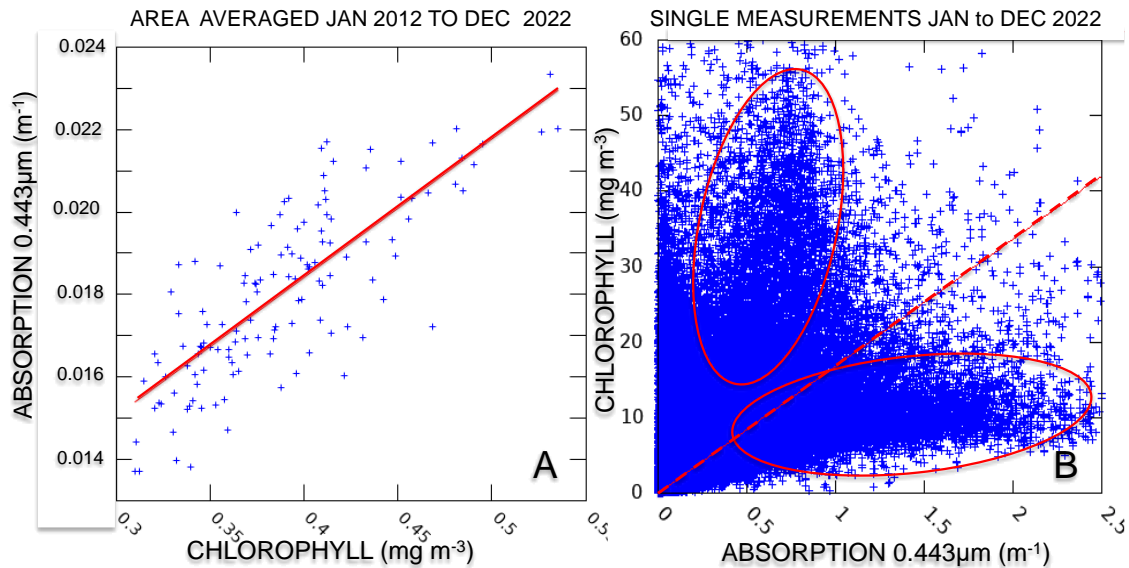


Figure 8: Comparison of chlorophyll and absorption coefficient at $0.443\mu\text{m}$ in region 80°W , 10°S to 20°E and 25°N , site 1 in Figure 1. A: Area averaged for chlorophyll and absorption coefficient at $0.443\mu\text{m}$, with correlation coefficient $R=0.78$, January 2012 to December 2022. B: Scatter diagram based on 12,031,604 data points for absorption coefficient and chlorophyll concentrations, January 2022 to December 2022. The straight line shows the linear regression and the correlation coefficient $R= 0.72$.

The seasonal changes of the mixed layer is shown in Figure 9, and it is evident that the shallowest depth is located along the equator where blooming is observed especially during June to August when variability of chlorophyll concentration is due to perturbations in the depth of the thermocline. It was pointed out that changes in the depth of the thermocline are induced by zonal wind anomalies in the western Tropical Atlantic beginning in July when zonal winds start weakening (Grotsky *et al.*, 2008) and the cold tongue extends into the equatorial region in a westward direction. The seasonal cycle of the mixed layer in the western Tropical Atlantic is also controlled by the surface freshwater flux while the seasonal cycle in the central Tropical Atlantic is predominantly controlled by precipitation (Da-Allada *et al.*, 2013).

Spectral signatures can be complementary to mixed layer depth, temperature and salinity that enhance the information content due to changes in chemical composition, species composition, depth location or concentrations in water. This is shown in Figure 10A with correlation images of chlorophyll and temperature and in Figure 10B with correlation for chlorophyll and the normalized fluorescence line height (NFLH). Figure 10A shows the far-reaching effect of the effluents from the Amazon and the Orinoco and on the eastern basin the effects from the Congo.

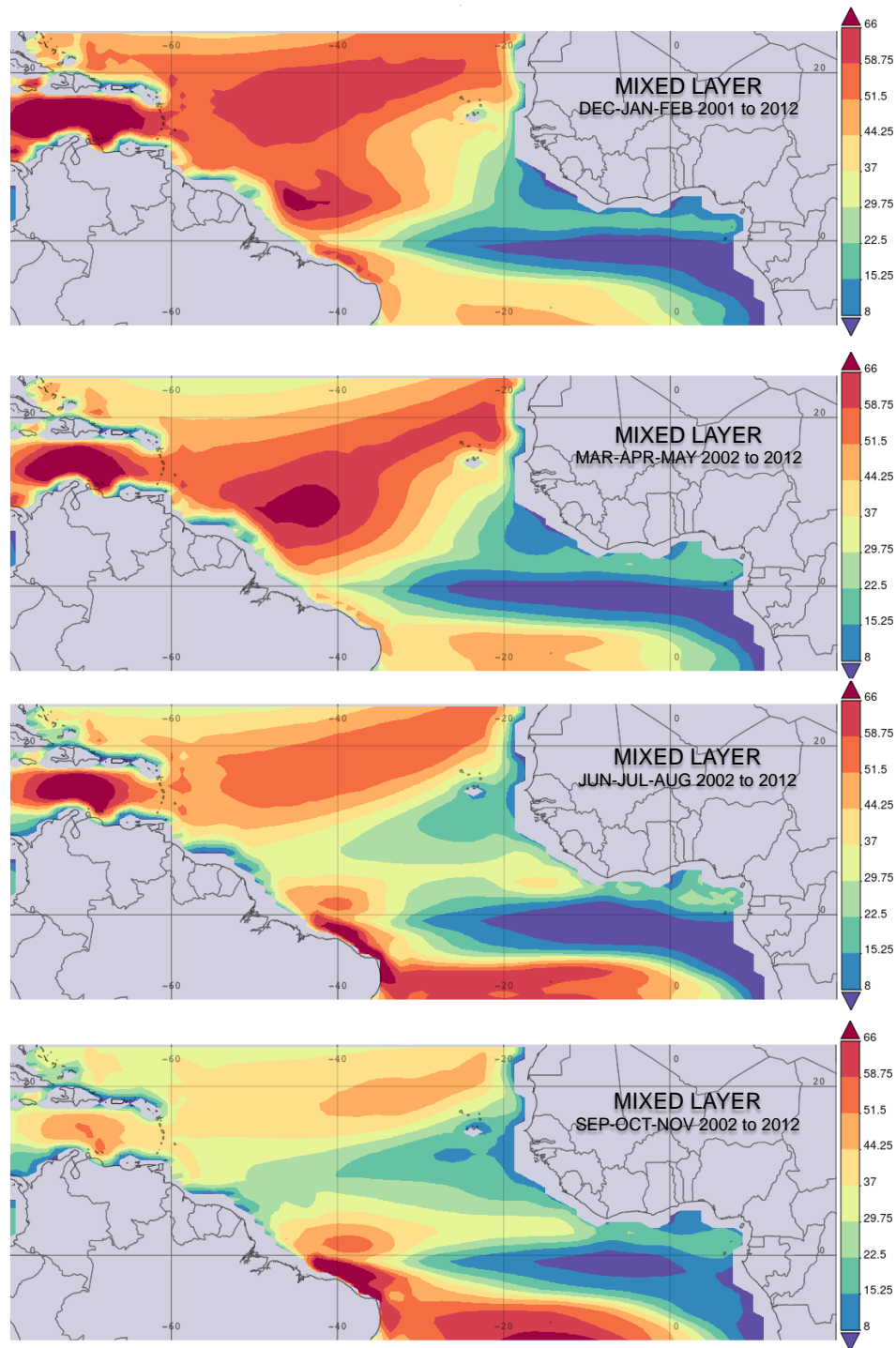


Figure 9: Depth of mixed layer (m) during different seasons based on monthly averaged measurements.

Negative correlations between temperature and chlorophyll are found in the upwelling areas where low temperatures are affiliated with high concentrations of chlorophyll. This is seen particularly in the

Research Article

equatorial region, at the coast of Columbia and Venezuela, along the northwest coast of Africa, and upwelling evident along the coast of Brazil.

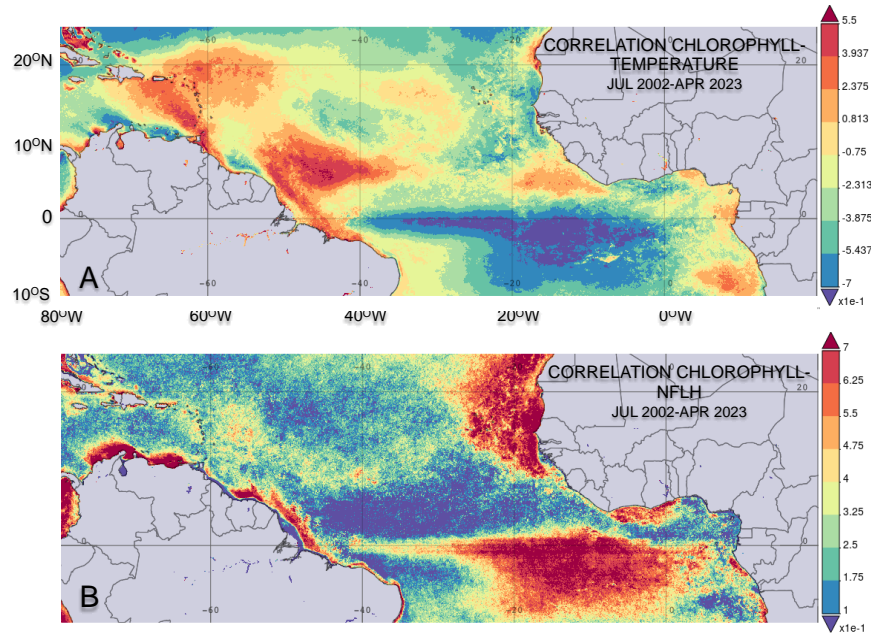


Figure 10: Correlation images July 2002 to April 2023. A: Correlation for chlorophyll and temperature; B: Correlation for chlorophyll and the normalized fluorescence line height (NFLH).

The correlation image of chlorophyll and the normalized fluorescence line height in Figure 10B discloses two dominant features that are annotated in red and blue. They can be explained by the dissimilar physiological state of phytoplankton populations and their different depth locations because the normalized fluorescence line height is retrieved from optical measurements at longer wavelengths compared to the retrieval of chlorophyll at shorter wavelengths. However, all correlation values are positive. The high correlation coefficient south of the equator is not fully resolved although a separate maximum is indicated farther south in Figure 10B with the correlation of chlorophyll and the normalized fluorescence line height.

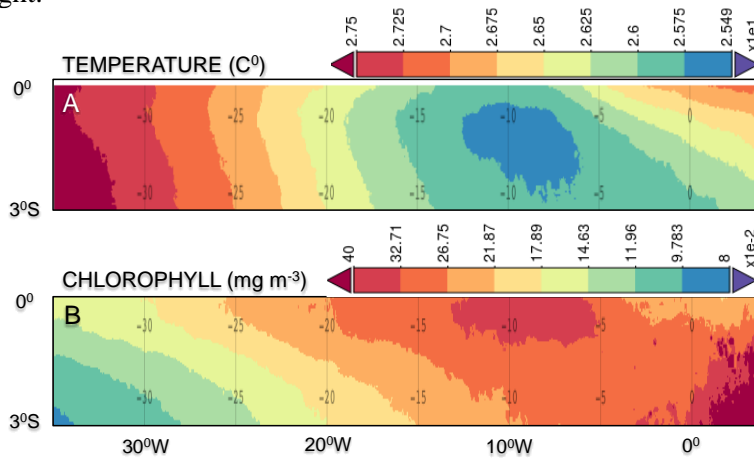


Figure 11: Averaged data for July 2002 to May 2023 at 35° W, 30°S to 4°E and Equator, A: Surface temperature (°C); B: Chlorophyll (mg m⁻³).

Research Article

The chlorophyll maximum and temperature minimum are further analyzed and are shown in Figures 11A and 11B that identify the location where elevated chlorophyll concentrations and low temperatures are found between the equator and 3°S at around 8°W. Low temperature and high chlorophyll coincide at the same longitude but the elevated chlorophyll concentrations are advected somewhat towards the equator that can be an indication of cross circulation at the surface of the nSouth Equatorial Current. The high concentrations of chlorophyll in the eastern region show that, based on the average of over two decades of data, the equatorial patch develops independently from the cold tongue in the east and is a result of equatorial upwelling. This can also be deduced from the average temperature field that demonstrates that the two regions of high chlorophyll concentrations are caused by two different mechanisms.

Interannual monthly means

The seasonal analysis of surface data suppresses many of the dynamic features in the tropical region when long-time data are averaged. However, observations at higher temporal resolution identify dynamics on a finer spatial scale that is documented in the following with monthly temporal resolution over a yearly cycle. The period January to February in Figure 12 is the season during which strong changes in chlorophyll are observed in the equatorial region but concentrations decrease during the period February/March. In May chlorophyll concentrations increase again until maximum levels are attained in June. Figure 13 shows that strong and persistent chlorophyll anomalies are observed in the western equatorial Atlantic by October and are explained by Chenillat *et al.*, (2021), with irregular wind divergence. The series of chlorophyll data show that wave structures start to be recognized in images in May/June and lasts until September, but due to the four-week average, the distribution structure becomes less distinct. The minimum in chlorophyll concentrations is observed in October until a second bloom develops in the equatorial region by November that lasts until January of the following year.

Fast changes in surface conditions of the Tropical Atlantic are known at various temporal levels during abnormally warm years in the eastern part of the cold tongue and abnormally cold boreal summers (Hormann and Brandt (2009). Anomalies in chlorophyll concentrations in the Tropical Atlantic are frequently a sign of vertical and horizontal dynamics within the upper water column that cause blooming events. Therefore, in addition to salinity and temperature distribution, chlorophyll data can add another dimension in recognizing the dynamic behavior of surface water. This is especially true for large-scale features like tropical instability waves that may frequently be encountered in different forms but are poorly resolved with monthly averaged data because averaging over one month distorts the apparent existence of waves. Waves that are connected to the South Equatorial Current are related to blooming events that are revealed with Hovmöller averaged chlorophyll and temperature data. Figures 14 A and B show the Hovmöller analysis for January 2020 to December 2022, while Figures 14C and 14D present an expanded time frame for January to December 2022. The comparison of temperature and chlorophyll in 2020 shows strong blooming in July that is in agreement with the distribution of cooler upwelled water in the equatorial region. Between October and January 2020 or 2022, the second blooming event is also recognized with temperature and chlorophyll, but concentrations are less pronounced compared to the summer bloom. In 2021/2022, the winter bloom is recognized with elevated chlorophyll concentrations of which the maximum is located at around 20°W although temperatures show only slight cooling. The following summer season in 2022, witnesses again lower temperatures with elevated chlorophyll concentrations, building a band that stretches from 5°E to 40°W. The expanded view of temperature and chlorophyll concentrations shown in Figures 14C and 14D shows the patchiness in chlorophyll distribution that drifts westward and is an effect of the tropical instability waves. Furthermore, the equatorial region experiences another blooming event that peaks around November to January the following year. This is the season during which tropical instability waves appear weaker although they can still be recognized in December.

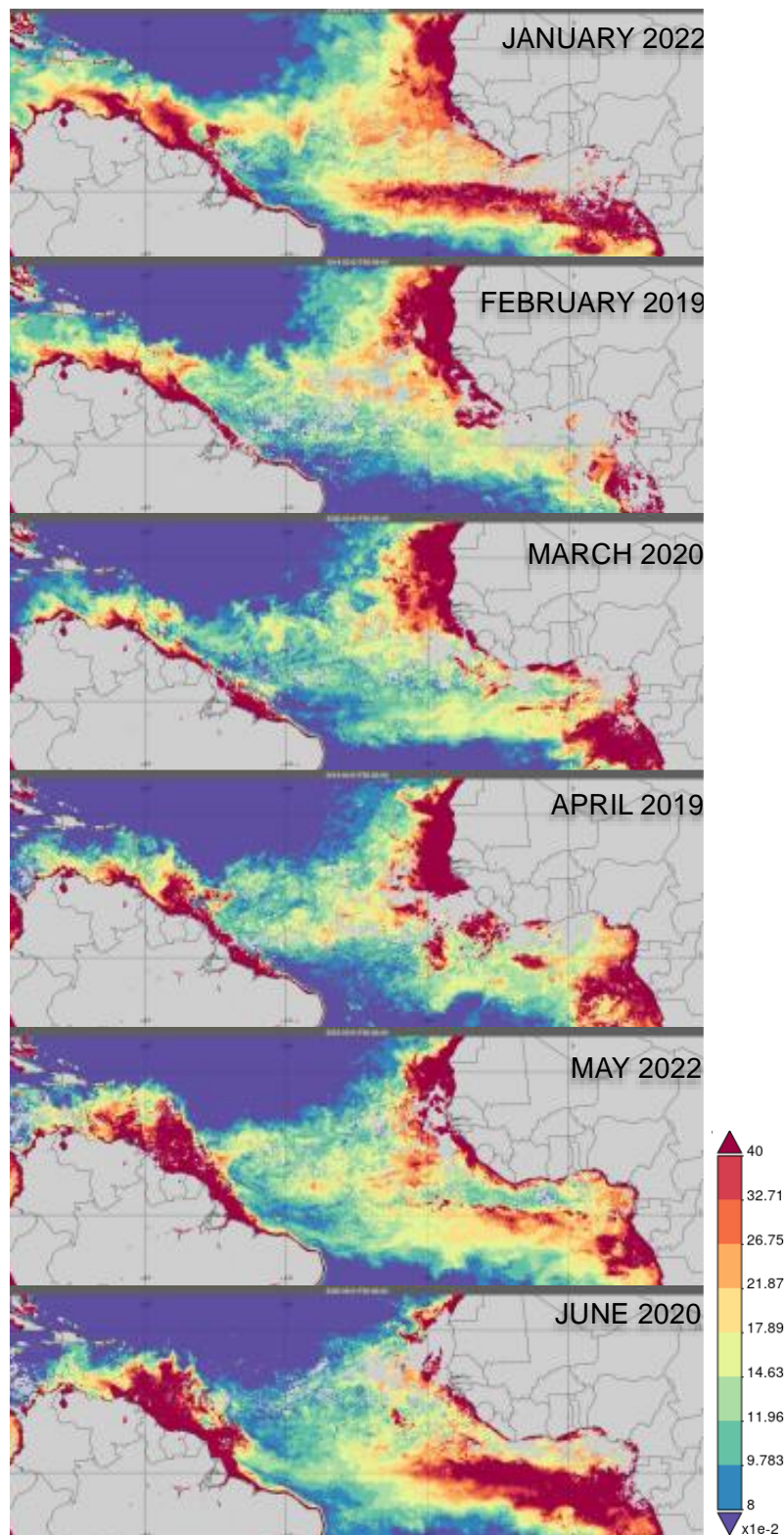


Figure 12: Monthly-averaged chlorophyll concentrations (mg m^{-3}) for January to June where the color scale refers to chlorophyll. Best images for 2022, and for months when clouds did not provide sufficient coverage, closest previous years (2019-2020) are identified.

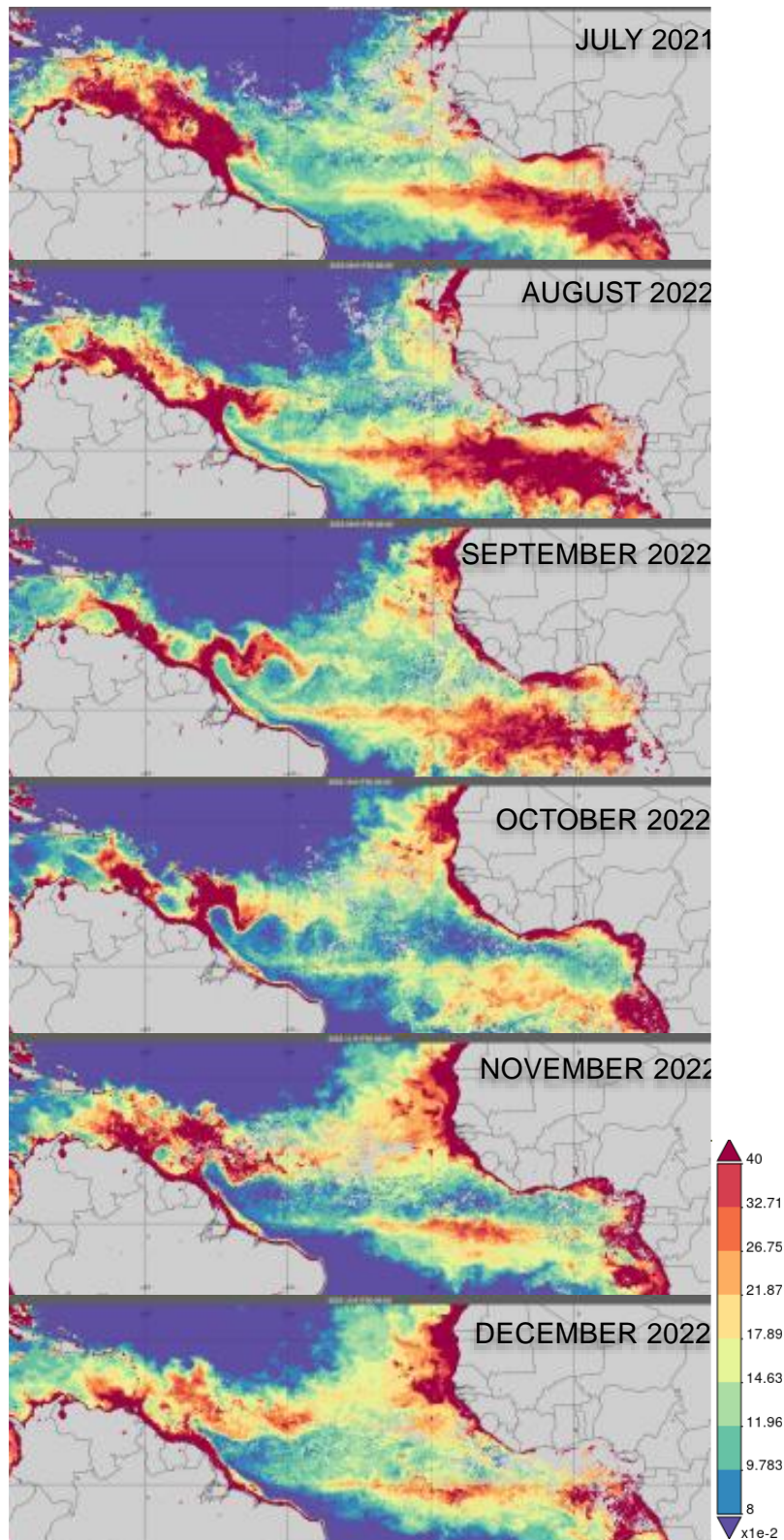


Figure 13: Monthly chlorophyll concentrations (mg m^{-3}). The color scale refers to chlorophyll. Images were selected from 2022, and when cloudfree data were not available in 2022, data from a previous year were included.

Research Article

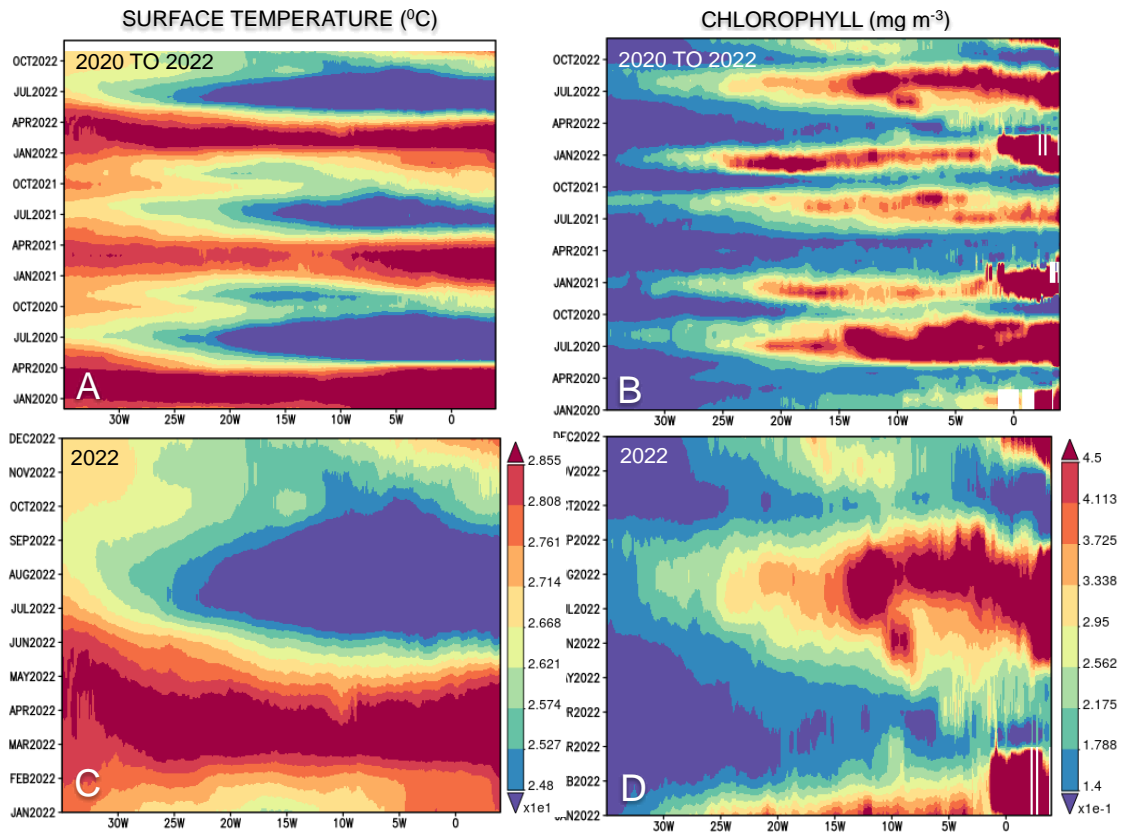


Figure 14: Hovmöller latitude monthly averaged chlorophyll and temperature data at site 35°W 3°S to 4°E 0°N. Figures A and B cover January 2020 to December 2022; C and D cover the expanded time for January to December 2022.

The region 35°W 3°S to 4°E 0°N (shown in Figure 1 as site 3) is displayed in Figure 15A as a scatter diagram comparing chlorophyll concentrations and temperature for the time frame July 2002 to May 2023. As the influence of costal water on chlorophyll concentration in this equatorial section is negligible, it is evident that the spikes are blooming events that emerge at specific temperature ranges. However, blooming does not always appear at the same temperature range as is indicated by the three blooming events at a temperature range between 21°C and 25°C, and the occurrence of blooming between 26°C and 30°C. This finding is in agreement with data presented in Figure 11 showing the location of two maxima in chlorophyll concentrations and their corresponding temperatures, and therefore heterogeneity and patchiness in the distribution of chlorophyll can be anticipated. This is indicated by the observations with clusters as shown in Figures 15B to 15E with scatter diagrams by comparing the absorption coefficient at 0.443µm and chlorophyll concentrations. They support the assumption that various ecosystems develop throughout the equatorial region and that they fluctuate with the seasons. The regression for the different seasons does not change substantially but an extreme clustering for October to December is seen when one cluster dominates that is recognized as a contributor to the clusters that are observed during the other seasons. The correlation during the summer bloom in July to September as shown in Figure 15D has the lowest correlation of $R = 0.76$ that indicates high variety in the data that can be caused by several factors including depth location of the bloom, specie variation, cell density as well as physiological condition of the primary producers.

Research Article

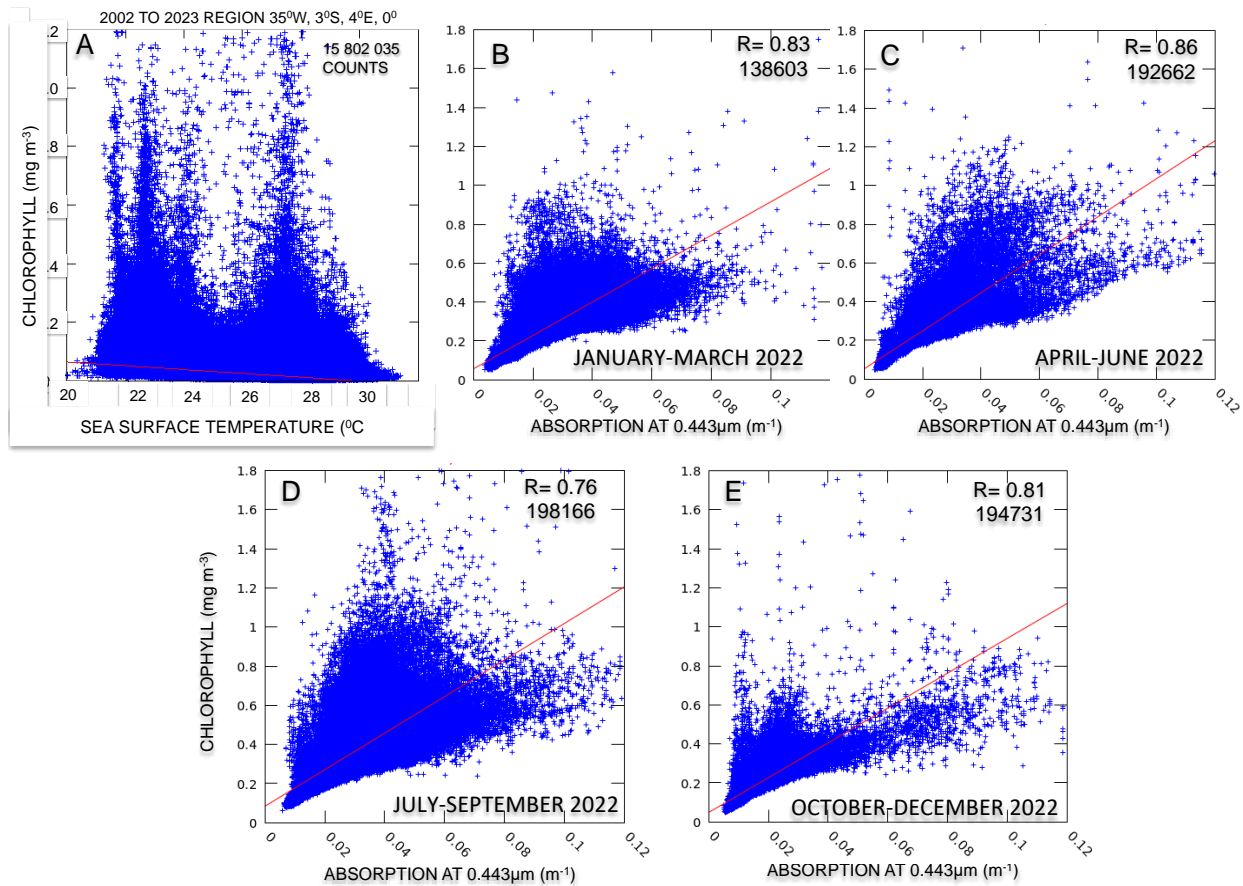


Figure 15: A: Scatter diagram for sea surface temperature and chlorophyll for July 2002 to May 2023. B to E: Scatter diagrams for the absorption coefficient at 0.443 μm (m⁻¹) and chlorophyll concentrations (mg m⁻³). The numbers below R are the numbers of data points. All graphs are derived from the same equatorial region as shown in Figure 1 with insert 3, located at 35°W 3°S to 4°E 0°N.

Tropical instability waves

The high variability in the Tropical Atlantic is characterized by the presence of westward propagating waves and eddies that are also linked to the North Brazil Current retroflexion (Mélise and Arnault, 2017; Johns *et al.*, 1990; Didden and Schott, 1993; Richardson *et al.*, 1994; Fratantoni *et al.*, 1995). Since waves are associated with horizontal and vertical advection, they provide additional nutrients for primary production. Therefore, fluctuating chlorophyll concentrations south of the equator may indicate tropical instability waves because they are associated with the vertical shear of the South Equatorial Current (von Schuckmann *et al.*, 2008). Instability waves appear also north of the equator at around 3°N to 7°N and between 50°W and 10°W that show strong seasonal cycling with maximum amplitude around August and propagate westward (Mélise and Arnault, 2017). However, tropical instability waves in the south of the Atlantic equator are not well documented, although instability waves seem to be present all year round and appear as cusp-like features. Their wavelengths may vary between 600 and 1200km with phase speeds between 20 and 50cm sec⁻¹ (Jochum *et al.*, 2004; Legeckis and Reverdin, 1987; Steger and Carton, 1991) and an estimated period of about 4 to 24 months (Charria *et al.*, (2006). However, their wavelengths and phase speed set a limit to their detection with monthly averaged data and therefore, a

Research Article

five-day binned data set was used. The recognition of instability waves with five day averaged chlorophyll data is demonstrated with a summer bloom shown in Figure 16. Wave appearance is recognized in both images, and comparing Figures 16A and 16B, derives a rough estimate of the wave progression in a westward direction of about 22 cm sec^{-1} and a wavelength of around 350 to 400km.

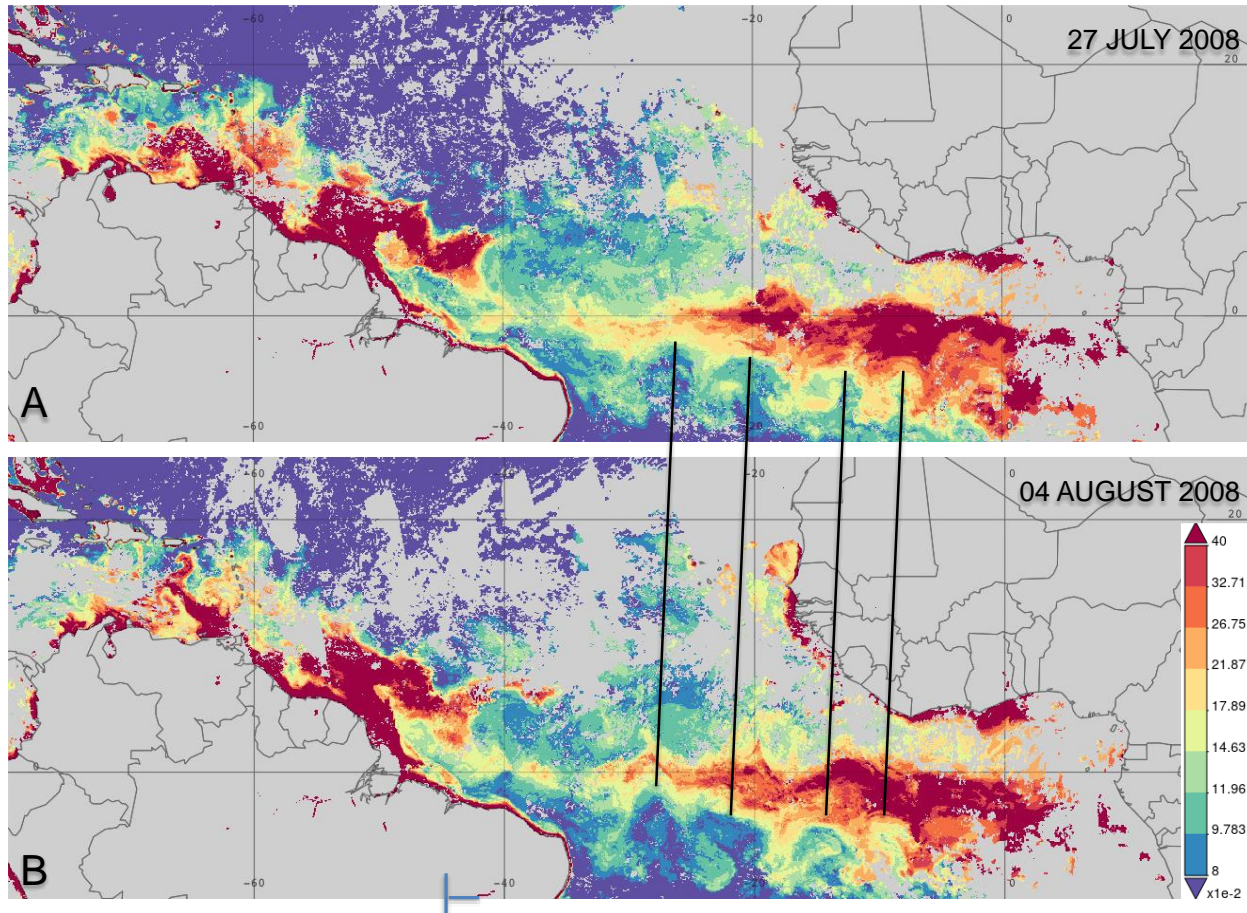


Figure 16: A: Chlorophyll concentrations for 27 July 2008; B: Chlorophyll concentrations for 4 August 2008 in the Tropical Atlantic. Each frame is based on a five-day composite of data. Values in the color code represent chlorophyll (mg m^{-3}). Note that the images have been selected according to their low cloud frequency, however there are still regions with missing data that are annotated as grey.

For comparison, temperature distribution pattern for the summer season is shown in Figure 17. Only eight-day averages were available in Giovanni but structures of tropical instability waves can still be recognized. However, the distribution pattern of temperature does not resolve instability waves as clearly as chlorophyll data do. An explanation could be the surface warming of cold upwelled water, whereas chlorophyll patterns remain to a high degree during warming. In addition, the temperature data are available at eight-day temporal resolution whereas chlorophyll was analyzed at five-day resolution, and temporal difference in binning data shows an effect on resolving the instability waves. As the waves progress at a speed of about 0.22 m sec^{-1} they would travel around 150 km within eight days, and as a result, binned data within this time would generate blurred gradients in images or even partly eliminate existing waves in images, through either subtraction or addition of waves.

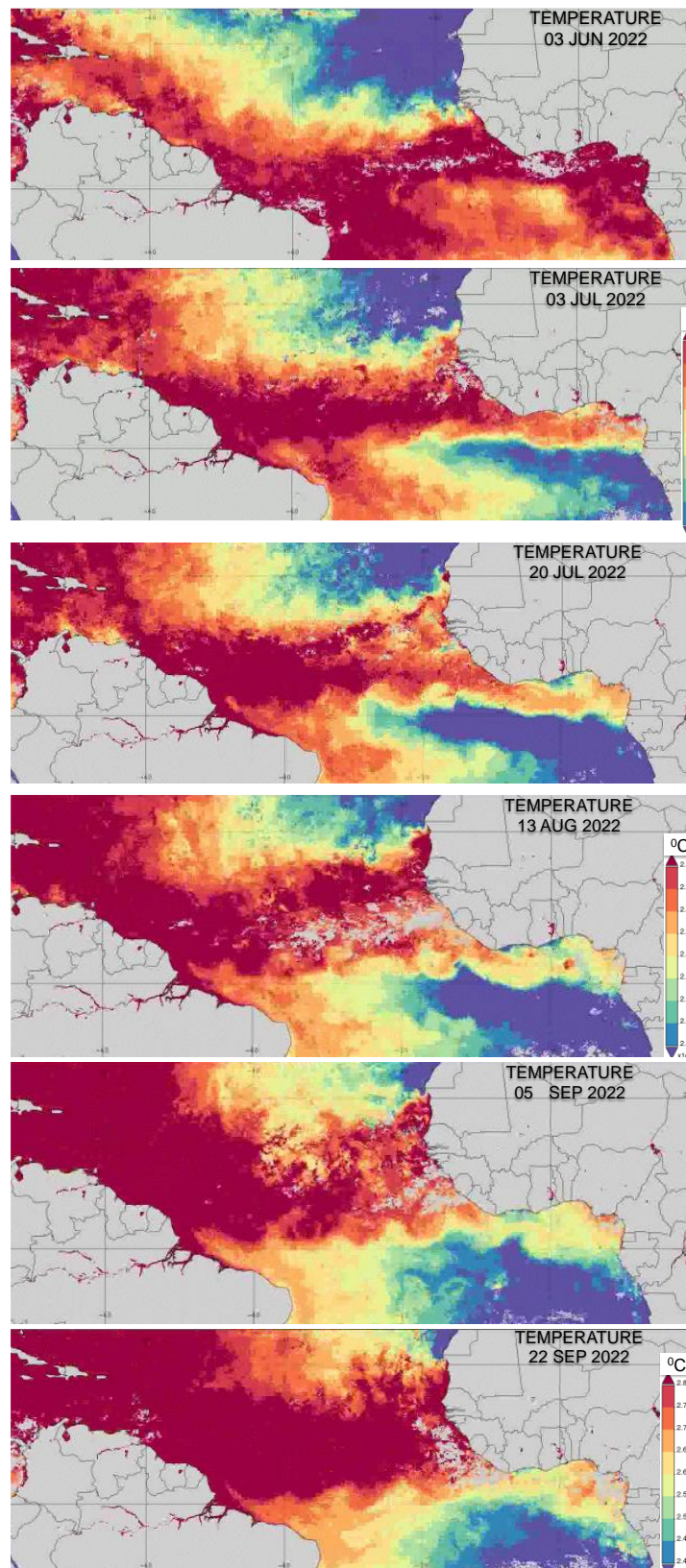


Figure 17: Sea surface temperature at eight-day resolution during summer.

Research Article

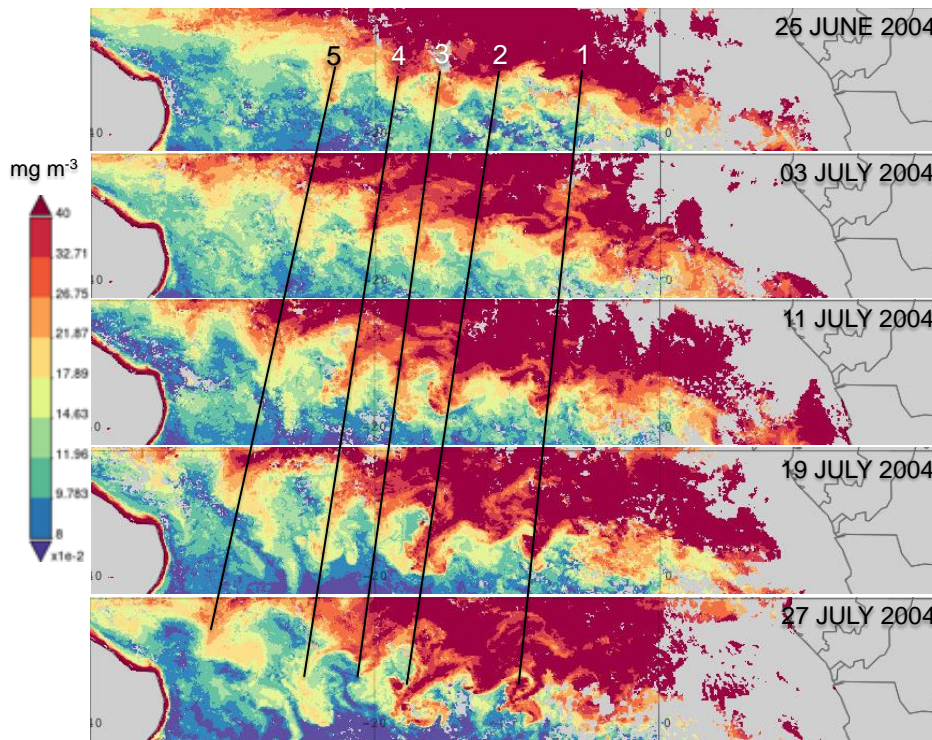


Figure 18: Chlorophyll distribution based on five-day composites for 26 June to 27 July 2004. The site covers 40°W, 10°S to 20°E, 0°N. Values in the color code represent chlorophyll (mg m^{-3}). Note that the images have been selected according to their low cloud frequency but areas of missing data are annotated as grey. The black lines 1 to 5 show the position where filaments and eddy formations are observed.

Tropical instability waves are present all year round and appear during the seasons with varying intensity but they are well developed during the summer season. Figure 18 provides evidence that during the progression of the waves from east to west, the wavelengths also increase as indicated by the positions of crest and troughs. The alteration of wavelength and phase speed is explained by the energy supply of the currents (Jocum *et al.*, 2004). The June/July period is the season during which chlorophyll reaches the maximum concentrations and separation of filaments from the waves are frequently observed. As is indicated in Figure 18, filaments also propagate towards the west but become eventually separated as individual eddies. However, once they are separated from the wake, they lose quickly their surface signatures in high chlorophyll concentrations. The changes of size and speed propagation of the wakes are part of the seasonal trend in the Tropical Atlantic and are confirmed for each year of which an example is given in Figure 19 where seasonal blooming and wave propagation are shown for the period 25 May to 26 June 2005. The formation of eddies separating from the edge of the waves are symptomatic events for this season and are tracked in this analysis over a period of four weeks. Development of eddies starts in the eastern part of the basin and the average chlorophyll concentration decreases towards the west. The white lines A to C in Figure 19 show the position where filaments and eddy building is in progress whereas the black lines 1 to 4 highlight the progression of waves, and lines B and C show the reduction of chlorophyll concentrations within four weeks once eddies are separated. The angle of the wave progression with respect to the equator seems to be almost constant during May and June and is included in Figure 19 as a black dashed line.

Research Article

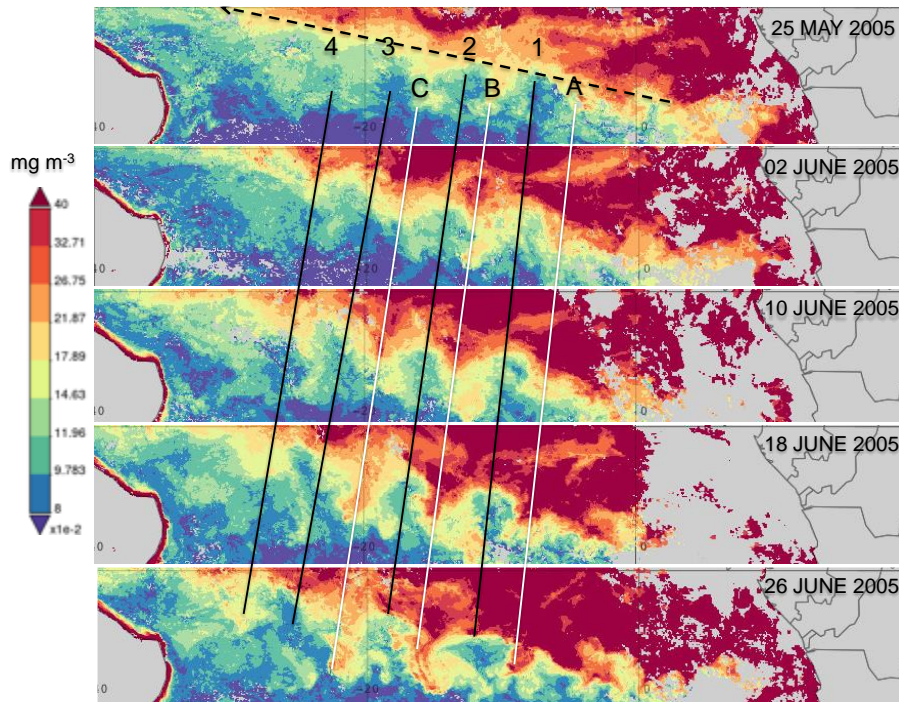


Figure 19: Chlorophyll distribution based on five-day composites for 25 May 2005 to 26 June 2005. The site covers 40°W, 10°S, to 20°E, 0°N and is seen in insert 2 of Figure 1. Values in the color code represent chlorophyll (mg m^{-3}).

The complexity and dynamics of the equatorial region make it attractive to examine the changes that may appear during a yearly cycle especially south of the equator. For this purpose, the least cloud covered regions were selected to analyze five-day binned data although the meteorological conditions restricted observations at the beginning of the year, but in May, however, useful data with low cloud coverage could be accessed. Figure 20 shows the increase of chlorophyll concentrations from east to west starting in May. Lines 1 to 4 indicate the location of eddy formation, and the sequence of images allows the tracking of eddies that separate from the waves. Line 2 demonstrates the building of an eddy that, based on chlorophyll distribution, seems to be initiated by cyclonic motion at the wave crest. The separation started on 17 May and the detachment of the eddy was completed on 8 June. Similar development of an eddy is marked by line 4. This eddy also has a significant cyclonic motion as derived from the sequence of chlorophyll distribution. It is observed that in general, the formation of eddies and their complete separation from the wave can be accomplished within a few weeks.

Blooming spreads during this season along the equator as seen with images in Figure 21 where line 1 emphasizes the development of a filament and line 2 is used as a reference to show that in relation to the other lines, the patchiness in chlorophyll concentrations is linked to wave propagation. Line 3 shows that eddy formation may occur within eight days and that separation from the wave starts with a cyclonic motion at the trough. The western part of the equatorial region shows a rather fuzzy distribution of chlorophyll that is an indication that during this season the current system may brake down to smaller eddies or gyres.

Cloudfree observations in August/September are limited especially in the eastern part of the basin. However, from the available data, it is also suggested that smaller eddies are generated. As seen in Figure 22, the cloud conditions did not improve from September to December. However, during this season, it is evident that concentrations of chlorophyll are lowered and that instability waves are absent or reduced.

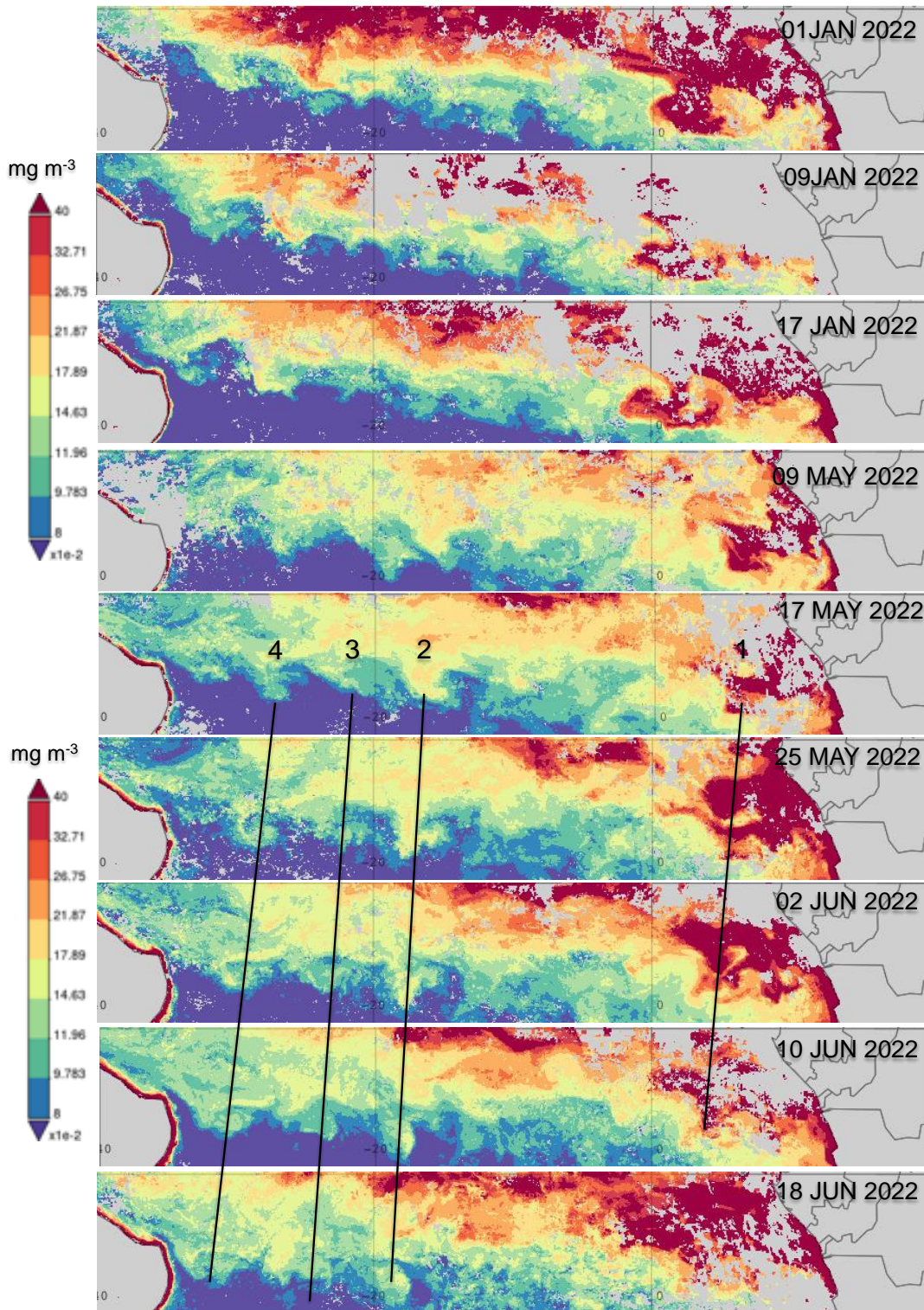


Figure 20: Chlorophyll distribution based on five-day composites for 1 January 2022 to 18 June 2022. The site covers 40°W, 10°S, to 20°E, 0°N and is seen in insert 2 of Figure 1. Values in the color code represent chlorophyll (mg m^{-3}).

Research Article

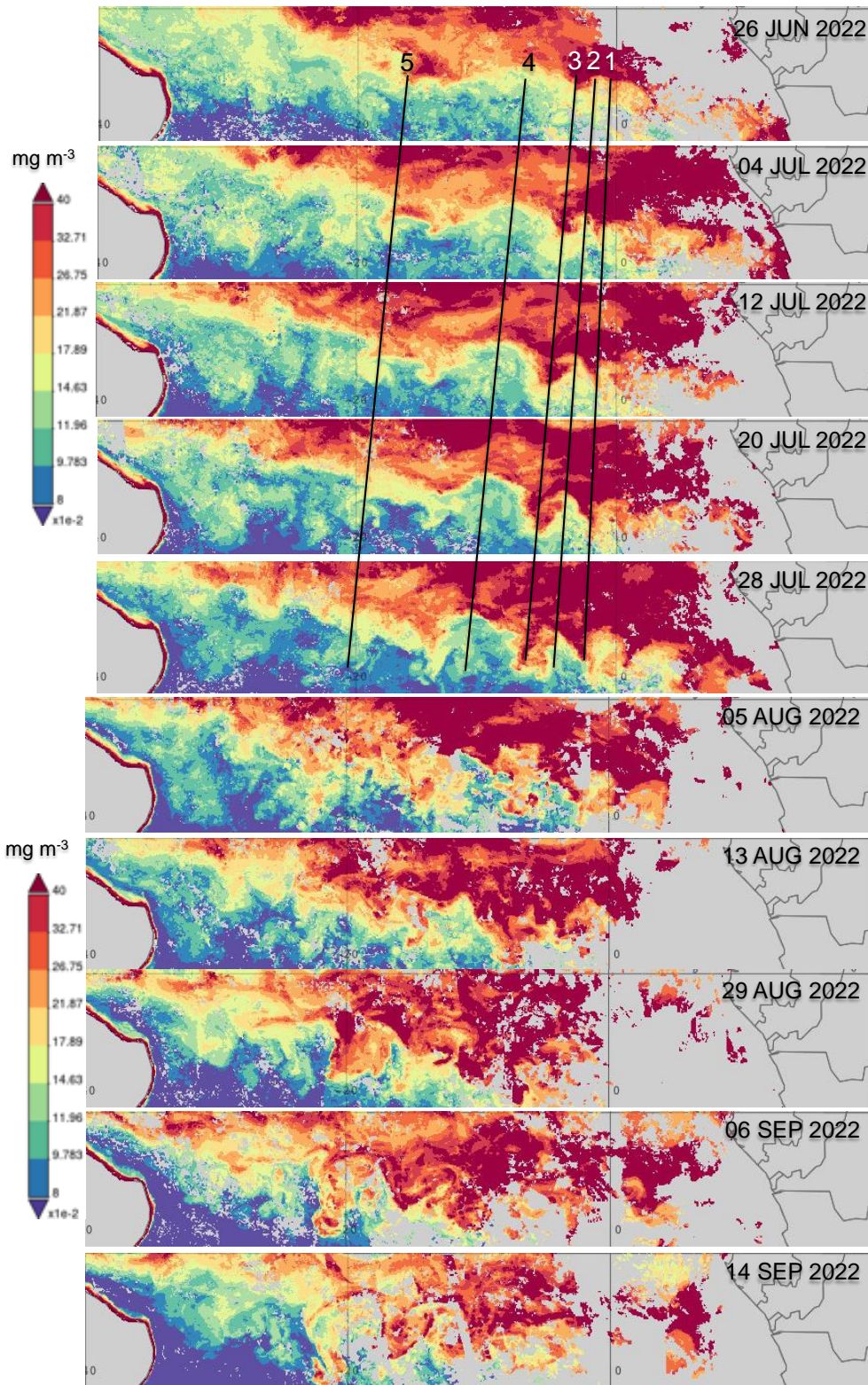


Figure 21: Chlorophyll distribution based on selected five-day composites for 26 June 2022 to 14 September 2022. The site covers 40°W, 10°S, to 20°E, 0°N and is seen in insert 2 of Figure 1. Values in the color code represent chlorophyll (mg m^{-3}).

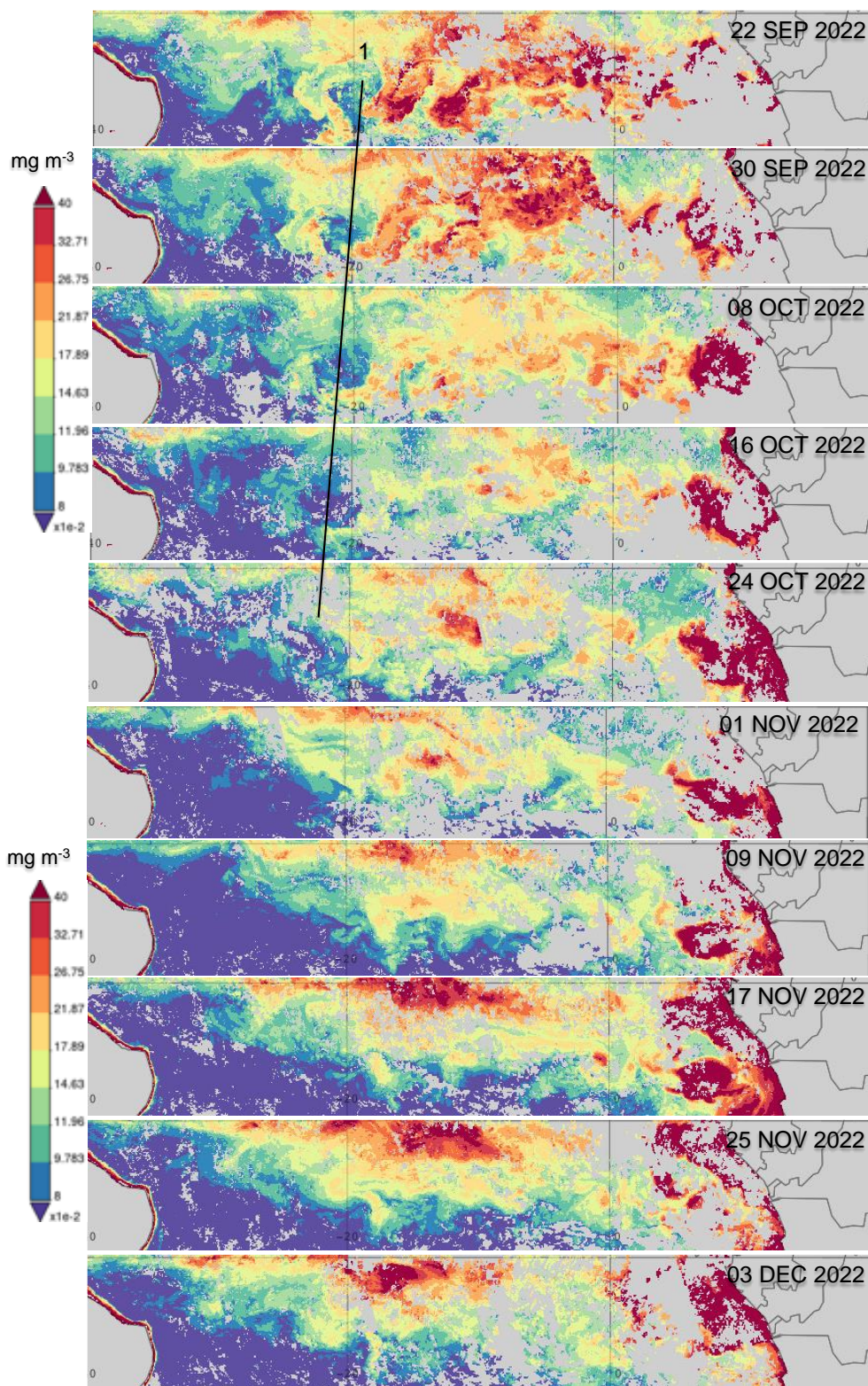


Figure 22: Chlorophyll distribution based on selected five-day composites for 22 September 2022 to 3 December 2022. The site covers 40°W, 10°S, to 20°E, 0°N and is seen in insert 2 of Figure 1. Values in the color code represent chlorophyll (mg m^{-3}).

Research Article

The yearly cycle of chlorophyll concentrations shows that in mid-summer cooling concurs with a chlorophyll maximum that can range in the average between 0.3 to 0.45 mg m⁻³. However, a second bloom starts to be recognized in November and this bloom is recognized with maximum chlorophyll concentrations in January of the following year. The second blooming in the equatorial region is recognized in Figure 23 with temperature measurements and chlorophyll concentrations. It shows that increasing temperature towards the winter season is interrupted around December with a slight cooling and coincides with the increase of chlorophyll. However compared to the summer blooming the winter bloom has in the average only chlorophyll concentrations between 0.18 to 0.39 mg m⁻³.

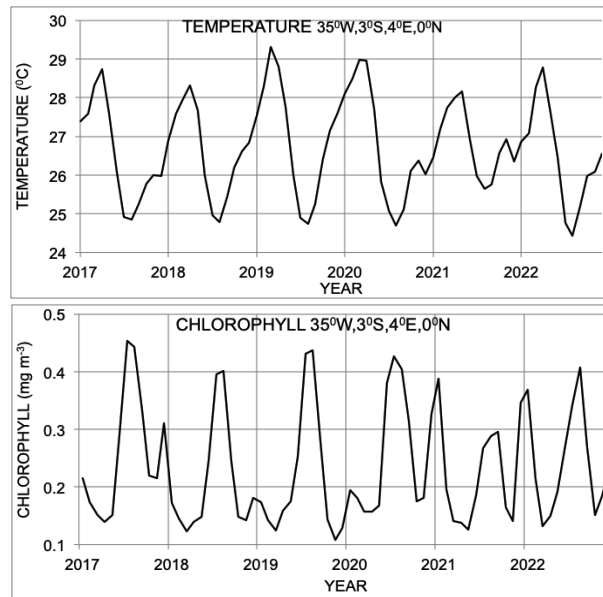


Figure 23: Time series of sea surface temperature and chlorophyll in the equatorial region at 35°W, 3°S to 4°E, 0°N, shown in Figure 1 as site number 3.

Longtime changes and trends in the equatorial region

Variability of chlorophyll concentration and its heterogeneous distribution patterns are frequently associated with temperature anomalies but changes may also appear at different time scales. Figure 24 documents changes of temperature and chlorophyll as obtained with time series from 2002 to 2022 in the equatorial region. Anomalous cooling is observed in 2011 and chlorophyll concentrations showed maxima in 2014/2015. In general, the fall/winter blooming undergoes strong fluctuations but blooming seems not always to be connected to lower temperatures, but general trends established with linear and polynomial regressions reveal long-term modulations of temperature and chlorophyll concentrations. The linear regression of the time series shows a steady increase of temperature, and a decrease in chlorophyll concentrations is detected. While short-ranging anomalies in the equatorial region are connected mainly to changes in the wind system and changes in the depth of thermocline (Hormann and Brandt, 2009; Pastor *et al.*, 2013), long-time observations show that changes in temperature and chlorophyll concentrations appear at various time scales and must be caused by a different mechanism. The polynomial fits suggest a rather large period of planetary waves passing through the equatorial basin in the Tropical Atlantic. The estimate provides a possible period of about 16 years. It can be expected that the stipulated multi-decadal modulation could cause increased vertical stratification in the water column and therefore could reduce nutrient support by increased vertical stratification due to global warming, as pointed out by Behrenfeld *et al.*, (2006). In addition to the effects of global temperature increase, are

Research Article

multi-decadal modulations that superimpose additional changes on the marine environment and would be in agreement with studies on interactions in climate systems, referred to as Atlantic Niño (Lübbecke *et al.*, 2018).

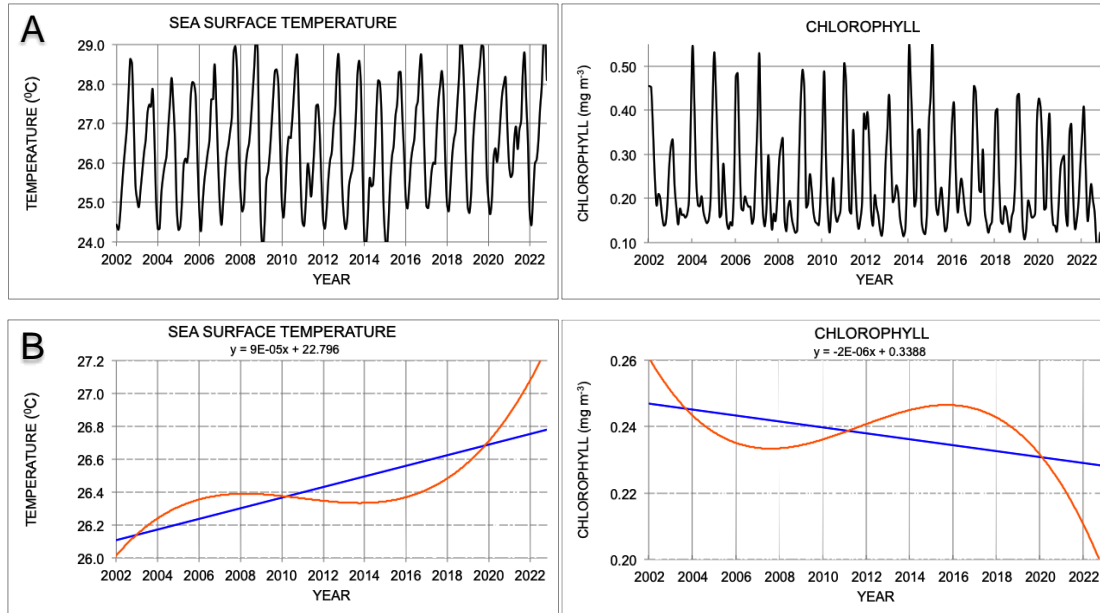


Figure 24: Averaged monthly temperature and chlorophyll concentration in the equatorial region at 35°W, 3°S to 4°E, 0°N, shown in Figure 1 as site number 3.

CONCLUSION

The image interpretation of the Tropical Atlantic shows the rather complex hydrography of the Tropical Atlantic. Long-time series of data that stretch over two decades allow the coverage of processes that appear at different temporal-spatial relationships. The grouping of observations into seasons demonstrates changes at course time scale during which current and atmospheric modulations occur. However, many of the surface manifestations in the tropical region are suppressed with long-time season averaged data, but correlation images yield a better delineation between different water masses and the presence of different marine ecosystems. This approach demonstrates that additional information can be extracted from climatic data, and structures can be recognized that would not be obtained from a single component interpretation.

The near-equatorial part of the Tropical Atlantic is characterized by the presence of westward propagating instability waves and eddies that are a major source of surface variability in chlorophyll. The waves have a progression at a velocity of about 22 cm sec⁻¹, and the wavelength is estimated to be in the average of around 350 to 400km. The observed formation and separation process of eddies from waves can be accomplished within three weeks. By mid-summer, cooling concurs with average chlorophyll concentrations reaching a maximum that may range between 0.3 to 0.45 mg m⁻³. Another blooming event peaks around November to January of the following year and is related to light cooling. Long-time observations show that changes in temperature and chlorophyll concentrations appear at various time scales with a rather long period, and it is suggested that planetary waves may pass through the equatorial basin in the Tropical Atlantic. The possible period is about 15 years and this would make it plausible that a variation of the thermocline goes parallel to the progression of a planetary wave and would initiate a modification of the marine ecosystem.

Research Article

ACKNOWLEDGEMENT

The author is affiliated with Ateneo University de Manila as Fulbright Alumnus and participates as International Faculty Member and is a Fulbright Alumnus at the University of the Bahamas. Analyses and visualizations used in this study were produced with the Giovanni online data system, developed and maintained by NASA GES DISC. The MODIS mission scientists and associated NASA personnel are acknowledged for the production of the data used in this research effort.

REFERENCES

- Acker JG and Leptoukh G (2007)**. Online analysis enhances use of NASA earth science data. *Eos, Transactions American Geophysical Union* **88** (2) 14–17. <https://doi.org/10.1029/2007EO020003>
- Amaya DJ, DeFlorio MJ, Miller AJ, and Xie S-P (2017)**. WES feedback and the Atlantic meridional mode: Observations and CMIP5 comparisons. *Climate Dynamics* **49** 1665-1679.
- Awo FM, Alory G, Da-Allada CY, Delcroix T, Jouanno J, Kestenare E, and Baloitcha E (2018)**. Sea surface salinity signature of the tropical Atlantic interannual climatic modes. *Journal of Geophysical Research: Oceans* **123** 7420–7437. <https://doi.org/10.1029/2018JC013837>
- Behrenfeld MJ, et al., (2006)**. Climate-driven trends in contemporary ocean productivity. *Nature* **444** 752– 755, doi:10.1038/nature05317
- Bischof B, Rowe E, Mariano AJ and Ryan EH (2004)**. The North Equatorial Current. *Ocean Surface Currents*. <https://oceancurrents.rsmas.miami.edu/atlantic/north-equatorial.html>
- Bonhoure D, Rowe E, Mariano AJ, Edward H. RyanmEH (2004)**. The South Equatorial Current. *Ocean Surface Currents*. (2004). <https://oceancurrents.rsmas.miami.edu/atlantic/south-equatorial.html>.
- Cabré A, Pelegrí JL, and Vallès-Casanova I (2019)**. Subtropical-tropical transfer in the South Atlantic Ocean. *Journal of Geophysical Research: Oceans* **124** 4820-4837.
- Charria G, Dadou I, Cipollini P, Drévilion M, De Mey P and Garçon V (2006)**. Understanding the influence of Rossby waves on surface chlorophyll concentrations in the North Atlantic Ocean. *Journal of Marine Research* **64** 43–71.
- Chenillat F, Illig S., Jouanno J, Awo FM, Alory G and Brehmer P (2021)**. How do Climate Modes Shape the Chlorophyll-a Interannual Variability in the Tropical Atlantic? *Geophysical Research Letters* **48**, e2021GL093769. <https://doi.org/10.1029/2021GL093769>.
- Condie SA (1991)**. Separation and recirculation of the North Brazil Current. *Journal of Marine Research* **49** 1-19.
- Da-Allada CY, Alory G, du Penhoat Y, Lestenare E, Durand F, Hounkonnou NM (2013)**. Seasonal mixed-layer salinity balance in the tropical Atlantic Ocean: Mean state and seasonal cycle. *Journal of Geophysical Research: Oceans* **118** (1) 332-345. <https://doi.org/10.1029/2012JC008357>
- Dessiera A and Dongu JR (1994)**. The sea surface salinity in the tropical Atlantic between 10° and 30°N-seasonal and interannual variations (1977-1989). *Deep-Sea Research I* **41** (1) 81-100.
- Didden N and Schott F (1993)**. Eddies in the North Brazil Current Retroflexion region observed by Geosat altimetry. *Journal of Geophysical Research* **98** (C11) 20121–20131.
- Fonseca CA, Goni GJ, Johns WE and Campus EJD (2004)**. Investigation of the North Brazil Current retroflexion and North Equatorial Countercurrent variability. *Geophysical Research Letters* **31** 121304 doi:10.1029/2004GL020054.
- Fratantoni DM, Johns WE, Townsend TL (1995)**. Rings of the North Brazil Current: their structure and behavior inferred from observations and a numerical simulation. *Journal of Geophysical Research* **100** (C6) 10633–10654.
- Fratantoni DM and Richardson PL (2006)**. The evolution and demise of North Brazil Current rings. *Journal of Physical Oceanography* **36** 1241-1264.

Research Article

- Garzoli S, Field A and Yao Q (2003).** North Brazil Current rings and the variability in the latitude of retroflexion. In: *Interhemispheric Water Exchange in the Atlantic Ocean*. Elsevier Oceanography Series 68: 357-373. DOI: [10.1016/S0422-9894\(03\)80154-X](https://doi.org/10.1016/S0422-9894(03)80154-X).
- Gordon AL, Giulivi, CF, Busecke J, and Bingham, FM (2015).** Differences among subtropical surface salinity patterns. *Oceanography* **28** (1) 32–39. <https://doi.org/10.5670/oceanog.2015.02>
- Grodsky SA, Carton JA, and McClain CR (2008).** Variability of upwelling and chlorophyll in the equatorial Atlantic. *Geophysical Research Letters*, **35**, L03610. <https://doi.org/10.1029/2007GL032466>.
- Gyory J, Mariano AJ, and Ryan EH (2004).** The Guiana Current. *Ocean Surface Currents*. <https://oceancurrents.rsmas.miami.edu/atlantic/guiana.html>.
- Hellweger FL and Gordon AL (2002).** Tracing Amazon River water into the Caribbean Sea. *Journal of Marine Research* **60** 537–549.
- Hopkins J, Lucas M, Dufau C, Sutton M, Stum J, Lauret O and Channelliere C (2013).** Detection and variability of the Congo River plume from satellite derived sea surface temperature, salinity, ocean colour and sea level. *Remote Sensing Environment* **139** 365-385. <https://doi.org/10.1016/j.rse.2013.08.015>
- Hormann V and Brandt P (2009).** Upper equatorial Atlantic variability during 2002 and 2005 associated with equatorial Kelvin waves. *Journal of Geophysical Research*, **114** C03007. <https://doi.org/10.1029/2008JC005101>.
- Hu C, Montgomery ET, Schmitt RW and Müller-Karger FE (2004).** The dispersal of the Amazon and Orinoco River water in the tropical Atlantic and Caribbean Sea: Observation from space and S-PALACE floats. *Deep-Sea Research Part II Topical Studies in Oceanography* **51** (10-11) 1151-1171 DOI:10.1016/j.dsr2.2004.04.001.
- Jochum M, Malanotte-Rizzoli P, Busalacci A (2004).** Tropical instability waves in the Atlantic. *Ocean Modelling* **7** 145-163. www.elsevier.com/locate/ocemod.
- Jochumsen K, Rhein M, Hüttl-Kabus S, and Böning CW (2010).** On the propagation and decay of North Brazil Current rings. *Journal of Geophysical Research* **115** C10004, doi:10.1029/2009JC006042.
- Johns WE, Lee TN, Schott FA, Zantopp RJ, Evans, RH (1990).** The North Brazil Current retroflexion: seasonal structure and eddy variability. *Journal of Geophysical Research* **95** (C12), 22103–22120.
- Legeckis R and Reverdin G (1987).** Long waves in the equatorial Atlantic Ocean during 1983. *Journal of Geophysical Research* **92** 2835– 2842.
- Liu Y, Cai W, Lin X, and Li Z (2022).** Increased extreme swings of Atlantic intertropical convergence zone in a warming climate. *Nature Climate Change* **12** 828–833.
- Liu Z and Acker J (2017).** Giovanni: The bridge between data and science. *Eos*, 98. doi. org/10.1029/2017EO079299
- Lübbecke JF, Rodríguez-Fonseca B, Richter I, Martín-Rey M, Losada T, Polo I, and N. S. Keenlyside NS (2018).** Equatorial Atlantic variability—Modes, mechanisms, and global teleconnections. *WIREs Climate Change* **9** e527 <https://doi.org/10.1002/wcc.527>
- Luko CD, da Silveira ICA, Simoes- Sousa IT, Araujo JM and Tandon A (2021).** Revisiting the Atlantic South Equatorial Current. *Journal of Geophysical Research: Oceans* **126** e2021JC017387. <https://doi.org/10.1029/2021JC017387>
- Martín-Rey M, Vallès-Casanova I, Pelegrí JL (2023).** Upper-Ocean Circulation and Tropical Atlantic Interannual Modes. *Journal of Climate* **36** (8) 2625–2643 <https://doi.org/10.1175/JCLI-D-22-0184.1>
- Mélice, J-L and Arnault S (2017).** Investigation of the intra-annual variability of the North Equatorial Countercurrent/North Brazil Current eddies and of the Instability Waves of the North Tropical Atlantic Ocean using satellite altimetry and empirical mode decomposition. *Journal Of Atmospheric And Oceanic Technology* **34** 2295 – 2310. doi: 10.1175/JTECH-D-17-0032.1.
- Müller-Karger FE, McClain CR and Richardson PL (1988).** The dispersal of the Amazon’s water. *Nature* **333** 56–59.

Research Article

Pastor MV, Palter JB., Pelegrí JL, Dunne JP (2013). Physical drivers of interannual chlorophyll variability in the eastern subtropical North Atlantic. *Journal of Geophysical Research: Oceans* **118** (8) 3871-3886. doi.org/10.1002/jgrc.20254.

Perez V, Fernandez E, Maranon E, Serret P, Garcia-Soto C (2004). Seasonal and interannual variability of chlorophyll-a and primary production in the Equatorial Atlantic: In situ and remote sensing observations. *Journal of Plankton Research* **27** (2) 189– 197.

Richardson PL, Hufford GE, Limeburner R, Brown WS (1994). North Brazil Current Retroflection Eddies. *Journal of Geophysical Research* **99** (C3) 5081–5093.

Richter I, Behera SK, Masumoto Y, Taguchi B, Sasaki H, Yamagata T, (2013). Multiple causes of interannual sea surface temperature variability in the equatorial Atlantic Ocean. *Nature Geoscience* **6** (1) 43-47.

Steger J and Carton J (1991). Long waves and eddies in the tropical Atlantic Ocean: 1984–1990. *Journal of Geophysical Research* **96** 15161–15171.

Szekielda KH (2022). Environmental Dynamics of Surface Water in the Caribbean Region. *International Journal of Geology, Earth and Environmental Sciences* **12** 160- 187. ISSN 2277-2081.

von Schuckmann K, Brandt P, Eden C, (2008). Generation of tropical instability waves in the Atlantic Ocean. *Journal of Geophysical Research* **113** C08034 doi:10.1029/2007JC004712.

Waliser DE and Jiang X (2015). TROPICAL METEOROLOGY AND CLIMATE. | Intertropical Convergence Zone In: *Encyclopedia of Atmospheric Sciences*, 2nd ed. 121-131.